Distinct anterograde trafficking pathways of BACE1 and amyloid precursor protein from the TGN and the regulation of amyloid-β production

Jing Zhi A. Tan, Lou Fourriere, Jingqi Wang, Franck Perez, Gaëlle Boncompain, Paul Gleeson

Distinct anterograde trafficking pathways of BACE1 and amyloid precursor protein from the TGN and the regulation of amyloid-β production

Jing Zhi A. Tan[1]*, Lou Fourriere[1]*, Jingqi Wang[1], Franck Perez[2], Gaelle Boncompain[2] and Paul A. Gleeson[1]

[1]The Department of Biochemistry and Molecular Biology and Bio21 Molecular Science and Biotechnology Institute, The University of Melbourne, Victoria 3010, Australia
[2] Dynamics of Intracellular Organization Laboratory, Institut Curie, PSL Research University, Sorbonne Université, Centre National de la Recherche Scientifique, UMR 144, Paris, France

(*) These authors contributed equally to this work

Running Title: Anterograde trafficking of BACE1 and amyloid production

Corresponding author: Prof. Paul Gleeson**,** Department of Biochemistry and Molecular Biology and Bio21 Molecular Science and Biotechnology Institute**,** The University of Melbourne**,** Victoria 3010**,** Australia
Phone 61-3-8344-2354: Fax 61-3-9348-1428, E-mail: pgleeson@unimelb.edu.au

Key words: anterograde transport, beta-secretase 1 (BACE1), small GTPase, Arf1, Arf4, AP-1, AP-4, amyloid precursor protein (APP), amyloid beta (Aβ), *trans*-Golgi network, membrane transport, primary neurons

Abbreviations: Aβ, beta-amyloid peptide; BACE1, beta site APP-cleaving enzyme; APP, amyloid precursor protein; AD, Alzheimer's disease; TGN, trans-Golgi network; RUSH, retention using selective hooks; ER, endoplasmic reticulum; GFP, green fluorescent protein; PM, plasma membrane; TfR, transferrin receptor; TIRF, total internal reflection fluorescence microscopy; DIV, day in vitro

Abstract

Processing of amyloid precursor protein (APP) by the β-secretase, BACE1, is the initial step of the amyloidogenic pathway to generate amyloid-β (Aβ). Although newly synthesised BACE1 and APP are transported along the secretory pathway, it is not known if BACE1 and APP share the same post-Golgi trafficking pathways or are partitioned into different transport routes. Here we demonstrate that BACE1 exits the Golgi in HeLa cells and primary neurons by a pathway distinct from the trafficking pathway for APP. Using the RUSH system, we show that BACE1 is transported from the TGN to the plasma membrane in an AP-1 and Arf1/4 dependent manner. Subsequently, BACE1 is endocytosed to early and recycling endosomes. Perturbation of BACE1 post-Golgi trafficking results in an increase in BACE1 cleavage of APP and increased production of both Aβ40 and Aβ42. These findings reveal that Golgi exit of BACE1 and APP in primary neurons is tightly regulated, resulting in their segregation along different transport routes, which limits APP processing.

Introduction

BACE1 is the primary β-secretase for initiating the β-site cleavage of amyloid precursor protein (APP) to generate the membrane-bound C99 fragment (Hussain *et al.*, 1999; Sinha *et al.*, 1999; Yan *et al.*, 1999; Bennett *et al.*, 2000). The subsequent cleavage of C99 by γ-secretase leads to the release of the pathogenic amyloidogenic Aβ peptide associated with Alzheimer's disease (Qi-Takahara *et al.*, 2005; Takami *et al.*, 2009; Tomita, 2014). BACE1 cleavage of APP is the rate-limiting step along the amyloidogenic processing pathway (Thinakaran and Koo, 2008; Zhang *et al.*, 2011) and, as both BACE1 and APP are membrane proteins, APP processing requires the convergence of these proteins to the same compartment (Kinoshita *et al.*, 2003). Hence, the intracellular trafficking and localization of BACE1 is coordinated with the processing of APP and biogenesis of Aβ peptides.

As a type-1 transmembrane aspartyl protease, BACE1 activity is optimal at acidic pH (Shimizu *et al.*, 2008), which is consistent with highest BACE1 activity detected in acidic compartments along the secretory and endocytic pathways including the endosomes and *trans*-Golgi (Bennett *et al.*, 2000; Huse *et al.*, 2000; Huse *et al.*, 2002; Toh *et al.*, 2017; Toh *et al.*, 2018). Modification to the trafficking and subcellular localization of BACE1 within these compartments is likely to impact upon APP processing. Indeed, previous work from our laboratory has shown that redirecting the BACE1 plasma membrane recycling pathway via the *trans*-Golgi network (TGN),

using a chimeric BACE1/TGN38 construct (TGN38 is known to traffic from the endosomes to the TGN), leads to an increased Aβ production (Chia *et al.*, 2013). Moreover, an extended residency time of BACE1 at the early endosomes also leads to an increase in Aβ production (Toh *et al.*, 2018). These studies highlight the importance of the TGN and early endosomes in APP processing and indicate that both the itinerary and kinetics of transport are relevant for regulating amyloidogenic processing. The intracellular itinerary of internalized BACE1 to the early endosomes followed by the recycling of BACE1 back to the plasma membrane (PM) via the recycling endosomes has been previously established (Chia *et al.*, 2013; Toh *et al.*, 2018). However, the post-Golgi trafficking of newly synthesized BACE1 is poorly defined yet is likely to play a critical role in initiating the production of Aβ peptides in the TGN. The TGN is a major sorting compartment of the cell and is responsible for transport of newly synthesised membrane proteins to a variety of different destinations (De Matteis and Luini, 2008), hence the transport pathway of BACE1 from the Golgi is defined by the sorting events in the TGN.

We have previously shown that newly synthesized APP traffics directly from the TGN to the early endosomes, a transport step regulated by the adaptor, AP-4, and the small G protein Arl5b (Burgos *et al.*, 2010; Toh *et al.*, 2017). The depletion of either Arl5b or AP-4 lead to the accumulation of APP, but not BACE1, in the TGN. Arl5b/AP-4 depletion also resulted in an increase in APP processing by endogenous BACE1, highlighting the importance of the TGN as a site for APP processing. As the post-Golgi export of BACE1 is independent of the Arl5b/AP-4 sorting pathway, the question arises as to the identity of the transport pathway(s) used by BACE1. The use of different pathways by BACE1 and APP (Toh *et al.*, 2017) could provide a mechanism to segregate BACE1 and APP within the TGN and to limit Aβ biogenesis.

Here we sought to define the post-Golgi export pathway of BACE1 and identify the sorting machinery involved. We have demonstrated that newly synthesized BACE1 traffics from the TGN directly to the cell surface. The adaptor AP-1 is not usually considered relevant for transport from the TGN to the cell surface. However, we considered this possibility as we identified a previously uncharacterized acidic cluster sorting signal in the cytoplasmic tail of BACE1. Moreover, the μ1 subunit of adaptor protein complex AP-1 was recently discovered to recognise an acidic cluster motif in the cytoplasmic tail of the model membrane cargo, CD8-furin (Navarro Negredo *et al.*, 2017). As AP-1 is localized at the TGN we therefore investigated whether AP-1 may regulate the post-Golgi trafficking of BACE1. We have demonstrated that AP-1 and the Arf small G proteins, Arf1 and Arf4, are required for efficient Golgi export of BACE1 in both HeLa cells and primary

neurons. Our findings also demonstrate that the segregation of BACE1 and APP into distinct pathways at the TGN is relevant to the regulation of APP processing and Aβ production.

Results

Trafficking itinerary of newly synthesized BACE1 from the TGN

It is currently not known if newly synthesised BACE1 shares the same post-Golgi trafficking route as APP or is segregated into a different transport pathway. The regulation of post-Golgi transport of BACE1 is likely to play a critical role in initiating the processing of APP and Aβ biogenesis. To analyze the anterograde transport of newly synthesized BACE1 from the Golgi complex, we utilized the Retention Using Selective Hooks (RUSH) system (Boncompain *et al.*, 2012; Boncompain and Perez, 2012). The bicistronic BACE1 RUSH plasmid contains BACE1 fused to the streptavidin-binding peptide (SBP) and a GFP tag and an ER-hook protein fused to streptavidin (Fig. 1A). Transiently expressed BACE1-SBP-GFP is retained in the ER compartment via interaction of its SBP with the streptavidin fused ER-hook protein. Upon the addition of biotin, BACE1-SBP-GFP is released from the hook, thus allowing for ER exit of newly synthesized BACE1-SBP-GFP (Fig. 1A). The intracellular itinerary of newly synthesized BACE1-SBP-GFP in intracellular compartments was tracked in HeLa cells by fixing the cells at various time points after the addition of biotin and stained with different organelle-specific markers (Fig. 1A–C).

In the absence of biotin, BACE1-SBP-GFP displayed ER-like staining pattern (Fig. 1B), which overlapped substantially with the ER-marker, KDEL (Fig. S1A), limited overlap (<5%) with other organelle markers (Fig. 1B & C), and no overlap with a plasma membrane marker (Fig. S1B), indicating that newly synthesized BACE1-SBP-GFP was successfully retained in the ER. After 10 min incubation with biotin, BACE1-SBP-GFP exhibited a juxtanuclear staining pattern with very little overlap with the ER marker KDEL (Fig. S1A) or endosomal markers (Fig. 1C, Fig. S1C) and with 11.5 $\pm$ 3.5% of BACE1-SBP-GFP colocalized with the TGN marker, GCC88 (Fig. 1C, Fig. S1D), indicating arrival of the cargo at the Golgi from the ER. At 20 min, 43.8 $\pm$ 5.4% of BACE1-SBP-GFP overlapped with the TGN marker, GCC88, and showed minimum overlap (<5%) with the endosomal/lysosomal markers, EEA1, Rab11, and CD63 (Fig. 1B & C), indicating that a substantial percentage of BACE1-SBP-GFP had arrived at the TGN but not trafficked to other intracellular compartments.

At the 30 min time point, the level of BACE1-SBP-GFP which co-localised with the TGN marker had decreased to 21.7 $\pm$ 4.1%, whereas there was an increase in BACE1-SBP-GFP in the

early endosome (16.7 ± 2.4%), marked by EEA1, and in the recycling endosome (11.7 ± 1.9%) (Fig. 1C and Fig. S1E). These data show that after 30 min of biotin addition, BACE1-SBP-GFP had begun to exit the TGN, and some cargo had arrived at the early and recycling endosomes. Given that BACE1 does not utilize the AP-4/Arl5b mediated TGN to early endosome trafficking pathway (Toh *et al.*, 2017), it is unlikely that newly synthesized BACE1-SBP-GFP traffics from the TGN directly to the early endosome. Rather, the BACE1-SBP-GFP detected in the early endosomes at 30 min likely represents the arrival of internalized BACE1 from the PM. On the other hand, the BACE-SBP-GFP in the recycling endosomes at 30 min may represent either direct trafficking of BACE1 from the TGN to the recycling endosomes or, alternatively, arrival of recycled BACE1 from the early endosomes (Chia *et al.*, 2013; Toh *et al.*, 2018).

After 45 and 60 min time points, the co-localization of BACE1-SBP-GFP with the early endosome (EEA1) marker remained steady at ~ 20 %, while the level of BACE1-SBP-GFP increased in the recycling endosome to 25.9 ± 2.1% by 60 min (Fig. 1B & C, Fig. S1E). On the other hand, the level of BACE1-SBP-GFP in the TGN decreased to 15.1 ± 2.5% at 45 min and 11.7 ± 2.2% by 60 min (Fig. 1B & C Fig. S1E). Thus, the majority of BACE1-SBP-GFP had exited the TGN by 45–60 min and is not recycled back to this compartment. Furthermore, the intracellular levels of BACE1-SBP-GFP in the early endosomes and recycling endosomes at the 60 min time point are very similar to the steady-state distribution of BACE1, as quantified from transfected cells incubated in continuous presence of biotin (Fig. 1C), indicating that the wave of BACE1 cargo from the ER had established an equilibrium throughout the cell by 60 min. There were low levels of BACE1-SBP-GFP (10.2 ± 2.3%) in CD63 positive late endosome/lysosome at both the 45 and 60 min time points (Fig. 1B & C; Fig. S1E), suggesting turnover of BACE1 in the lysosomes (Ye and Cai, 2014; Feng *et al.*, 2017; Ye *et al.*, 2017).

To directly analyze the arrival of newly synthesized BACE1-SBP-GFP at the PM, total internal reflection fluorescence microscopy (TIRF) was performed. BACE1-SBP-GFP at the PM was first detected at 22 min after biotin addition followed by a rapid increase in BACE1-SBP-GFP arriving at the PM (Fig. 2A & movie S1). This data is consistent with kinetics of BACE1-SBP-GFP exiting the TGN between the 20 min and 30 min time point (Fig. 1B & C, Fig. S1E). We then performed live-cell imaging with fast image acquisition to determine whether BACE1-SBP-GFP is delivered directly to the PM from the TGN or indirectly via recycling endosomes. Temporal projection of the BACE1-SBP-GFP signal shows a direct transport from a juxtanuclear compartment, likely to represent the Golgi compartment, directly to the distal edge of the cell after

20 to 30 min biotin addition (Fig. 2B & movie S2). Taken together, TIRF and fast acquisition imaging data indicate that newly synthesized BACE1 traffics directly from the TGN to the PM.

Steady-state distribution of BACE1 in HeLa cells and primary neurons

To identify the sorting machinery required the post-Golgi trafficking of BACE1 to the PM, it was important to analyze homogenous populations of cells expressing only modest levels of BACE1. As endogenous BACE1 in HeLa cells is very low and difficult to detect by immunofluorescence, a HeLa cell line stably expressing BACE1-GFP (HeLa-BACE1-GFP) was generated. A cell line (D5), expressing modest levels of BACE1-GFP was selected by cell sorting and cloning. HeLa D5 maintained BACE1-GFP expression over multiple passages and was used for the subsequent experiments.

We initially established the steady-state distribution of BACE1-GFP in HeLa-BACE1-GFP cells. BACE1-GFP was largely juxtanuclear with punctate-like structures throughout the cytoplasm (Fig. 3A). Dual staining showed an extensive overlap of BACE1-GFP with Rab11-positive recycling endosomes and only a low level of overlap with the TGN marker, GCC88, (Fig. 3A). Minimum overlap was detected between the Rab11 and GCC88 markers in HeLa cells (Fig. S2A), demonstrating that the majority of juxtanuclear BACE1-GFP was indeed localized to recycling endosomes. Quantitation of the steady-state distribution of BACE1-GFP revealed that 8.5 $\pm$1.8% localised with GCC88-marked TGN, 30.6 $\pm$ 3.6% localised with the Rab11-marked recycling endosomes, 27.4 $\pm$ 2.7% localised with the EEA1-marked early endosomes, and 9.7 $\pm$ 2.5 % in the CD63-positive late endosomes/lysosomes (Fig. 3A, B). This distribution of BACE1-GFP is very similar to the steady-state distribution of transiently expressed untagged-BACE1 in HeLa cells (Chia *et al.*, 2013) and to the distribution of BACE1-SBP-GFP in the RUSH system in the continuous presence of biotin (Table 1).

To determine if the intracellular distribution of BACE1 observed in transfected HeLa cells was consistent to the distribution of BACE1 in primary neurons, we next determined the distribution of endogenous BACE1 in mouse primary cortical neurons. The TGN and recycling endosomes in primary neurons are located in close physical proximity and concentrated in the juxtanuclear position of the soma (Fig. S2B). To determine if there is any overlap between these organelle markers we treated neurons with nocodazole, to disperse the Golgi, and stained the treated cells with the TGN markers (GCC88 and golgin245/p230) and the recycling endosome marker, Rab11. The markers recognised distinct structures with only minimum overlap (Fig. S2C),

demonstrating they were selective for each organelle. The majority of endogenous BACE1 co-localised with Rab11 and the early endosome marker, Rab4, and lower levels of endogenous BACE1 were detected in the late endosomes/lysosomes and Golgi (Fig. 3C, D). Although the percentage of BACE1 in each compartment show some differences between neurons and HeLa cells (Table 1), this data demonstrates that HeLa cell lines and the BACE1 RUSH system faithfully reflect the distribution of endogenous BACE1 in primary neurons.

AP-1 is required for the post-Golgi sorting of BACE1 in HeLa cells

Next, we sought to identify adaptor protein(s) that could regulate the post-Golgi transport of BACE1. In the cytoplasmic tail of BACE1, we come across a previously undetected acidic cluster sequence, DDFADDISLL, a motif presenting an extension of the previously defined DDISLL and DISLL motifs which play a role in endocytosis and endocytic sorting (He *et al.*, 2002; He *et al.*, 2005; Toh *et al.*, 2018). This acidic cluster motif is similar to the acidic cluster sequences discovered in the cytosolic tail of cargoes such as furin (Voorhees *et al.*, 1995), carboxypeptidase D (Eng *et al.*, 1999), and the cation-independent mannose 6-phosphate receptor (Chen *et al.*, 1997) (Table 2). Given that AP-1 has been shown to be associated with sorting of proteins with acidic cluster sequences (Navarro Negredo *et al.*, 2017), we examined whether the depletion of AP-1 impacts on the post-Golgi export of BACE1. Moreover, as Golgi-localised γ-ear containing Arf binding proteins (GGAs) are also localized at the TGN and have been shown to play a cooperative/overlapping role with AP-1 (Doray *et al.*, 2002; Hirst *et al.*, 2012), the depletion of GGA1 was also performed. Immunoblotting showed that the levels of AP-1γ and GGA1 were depleted by >90% and >80%, respectively, in HeLa-BACE1-GFP treated with either AP-1γ or GGA1 siRNA (Fig. 4A). The depletion of AP-1γ resulted in an increase in the accumulation of BACE1-GFP in the juxtanuclear region that co-localizes extensively with the Golgi marker, golgin-97, compared with control siRNA treatment (Fig. 4C & D). As we have used different TGN markers throughout this study, due to compatibility of the primary antibodies in dual and triple labelling experiments, we also analysed the co-location of BACE1-GFP in control and AP-1γ siRNA treated cells using antibodies to GCC88. Similar findings were observed with either TGN marker, golgin-97 or GCC88 (Fig. S3A), and moreover, we observed a high level of co-localisation between the two TGN markers golgin-97 and GCC88, as expected at the resolution used (Fig. S3B).

Quantitative analyses revealed a 3.0-fold increase in co-localization of BACE1-GFP with the TGN marker, golgin-97 in AP-1γ depleted cells compared with control siRNA-treated cells

(Fig. 4D). Conversely, the depletion of AP-1γ resulted in a decrease of in the total cell pool of BACE1-GFP that overlapped with Rab11 (Fig. 5), a reduction of similar magnitude as the increase found in the TGN in AP-1 knockdown cells.

On the other hand, the level of BACE1-GFP at the TGN was not altered in GGA1 depleted cells (Fig. 4C & D). We have previously proposed that the Golgi export of BACE1 is independent of the AP-4/Arl5b sorting machinery utilized by APP (Toh *et al.*, 2017). As expected, the depletion of either AP-4 or Arl5b in HeLa-BACE1-GFP also did not alter the distribution of BACE1-GFP at the Golgi (Fig. 4A, B & C). Quantitative analyses showed no significant changes in GGA1, AP-4ε and Arl5b depleted cells (Fig. 4D). AP-4 was depleted by >90% in HeLa-BACE1-GFP treated with AP-4ε siRNA (Fig. 4A). As antibodies are not available to detect endogenous Arl5b, we tested the efficiency of Arl5b depletion in parallel in the same experiment by assessing the decrease in the level of GFP in HeLa cells stably expressing Arl5b(Q70L)-GFP (Fig. 4B), a GFP fusion with the constitutive active form of Arl5b. Previous studies showed that silencing of GFP-Arl5b is also a read out for the silencing of endogenous Arl5b (Houghton *et al.*, 2012). Collectively, these results revealed that AP-1 is specifically required for the export of BACE1 from the TGN, and that BACE1 and APP have distinct post-Golgi sorting machineries.

Endogenous BACE1 accumulates at the Golgi in AP-1 but not AP-4 depleted primary neurons

To determine if AP-1 is also required for the sorting of BACE1 from the TGN in a more relevant cell model, we assessed the impact of silencing AP-1 in primary mouse cortical neurons. Primary mouse cortical neurons were transduced with AP-1γ shRNA recombinant lentivirus to silence AP-1. Transduced neurons were detected by the expression of GFP. GFP-positive transduced neurons displayed reduced staining of AP-1γ as detected by confocal microscopy (Fig. S4). In addition, endogenous BACE1 staining displayed an increase in the co-localization with the TGN marker, p230/golgin-245, compared with non-transduced neurons (Fig. 6A). Quantitative analyses of fluorescent intensities of 3D projections revealed an increase in co-localization of BACE1 with the TGN marker, p230/golgin-245, from 10.4 $\pm$ 3.1% in non-transduced neurons to 25.2 $\pm$ 5.6% in AP-1 depleted neurons (Fig. 6B). On the other hand, following transduction of primary neurons with AP-4ε shRNA recombinant lentivirus (Fig. S4B), there was no significant change in the co-localization of BACE1 with the TGN marker in AP-4 depleted neurons (Fig. 6B). We also assessed whether the depletion of AP-1 in neurons impacted the export of APP from the TGN; depletion of AP-1γ in neurons did not alter the distribution of APP in the Golgi (Fig. 6C and D). Taken together, AP-1 depletion specifically retains BACE1 but not APP in the TGN.

AP-1 depletion reduced the exit rate of BACE1 from the Golgi

To directly examine the impact of AP-1 depletion on the kinetics of anterograde trafficking of newly synthesized BACE1 in HeLa cells, we used the RUSH system described above. HeLa cells were transfected with AP-1γ siRNA then transfected with the BACE1-SBP-GFP. Silencing of AP-4ε was also included for comparison. Live imaging showed the arrival of BACE1-SBP-GFP within the juxtanuclear Golgi region within 15 min after biotin addition. Whereas the majority of BACE1-SBP-GFP had exited the juxtanuclear Golgi region by 45 min in control and AP-4–depleted cells, considerable BACE1-SBP-GFP fluorescence was still retained in the Golgi in AP-1-depleted cells at 45 min and also at 60 min (Fig. 7 A & B).

To further quantify and compare the residency time of BACE1-SBP-GFP in the Golgi in each condition, the average fluorescence intensity of the Golgi area was measured over time for individual cells. The maximal Golgi intensity of BACE1-SBP-GFP and the corresponding time-point for the intensity to reach maximum was determined (Fig. 7C & D). There was no significant deviation between the groups, indicating that the level of BACE1-SBP-GFP expression was similar and the ER-to-Golgi trafficking of BACE1-SBP-GFP was not affected by the siRNA treatment (Fig. 7C & D). The Golgi exit rate of BACE1-SBP-GFP was calculated based on the slope of the curve in Fig. 7B (Fig. 7E). AP-1-depleted cells showed a 35% reduction in the slope compared with control and AP-4 siRNA treated cells (Fig. 7E). From these findings, we conclude that the Golgi exit of BACE1-SBP-GFP was delayed in AP-1 depleted cells compared with cells treated with either control or AP-4ε siRNA

Depletion of Arf small G proteins required for the membrane recruitment of AP-1 results in the accumulation of BACE1 but not APP in the TGN

Given that the recruitment of AP-1 to TGN membranes has been reported to be regulated by both Arf1 (Stamnes and Rothman, 1993; Le Borgne and Hoflack, 1997; Lee *et al.*, 2008) and Arf4 (Lowery *et al.*, 2013; Nakai *et al.*, 2013) small G proteins, we investigated whether these two Arfs are required for the post-Golgi export of BACE1. In cells treated with either Arf1 or Arf4 siRNA, the levels of Arf1 and Arf4 were depleted by >90% and >81%, respectively, as assessed by immunoblotting (Fig. 8A). In addition, the depletion of Arf1 resulted in an increase in Arf4 levels

by ~20%, consistent with a previous report (Reiling *et al.*, 2013) (Fig. 8A). The depletion of either Arf1 or Arf4 accumulated BACE1-GFP in the juxtanuclear region that co-localizes extensively with the Golgi marker, golgin-97, compared with control conditions (Fig. 8B). Quantitation revealed that there was an increase in the co-localization of BACE1-GFP and golgin-97 from 8.1 $\pm$ 2.1% in control cells to 21.1 $\pm$ 2.4% and 25.7 $\pm$ 2.9% in Arf1 and Arf4 depleted cells, respectively (Fig. 8D). Notably, the depletion of Arf4 resulted in a greater accumulation of BACE1-GFP at the TGN compared with the depletion of Arf1 (Fig. 8D). To exclude an off-target effect of Arf1 siRNA and Arf4 siRNA, wild-type mCherry-tagged Arf1 and Arf4 constructs were expressed in cells treated with Arf1 siRNA and Arf4 siRNA, respectively (Fig. 8B, E & F). Rescued cells were detected by mCherry expression. BACE1-GFP did not accumulate in the Golgi of cells expressing either the Arf1 and Arf4 rescue construct, confirming that the accumulation of BACE1-GFP in the TGN was specifically due to the depletion of Arf1 and Arf4 (Fig. 8B, E & F).

Given that Arf1 and Arf4 are closely related (Donaldson and Jackson, 2011), Arf1 and Arf4 may have overlapping functions. To investigate this possibility, both Arf1 and Arf4 were depleted simultaneously. The double knockdown of Arf1+Arf4 depleted Arf1 by 82% whereas Arf4 was depleted by only 55% as assessed by immunoblotting (Fig. 8A). A previous study showed that Arf1 depletion caused Arf4 levels to increase (Reiling *et al.*, 2013), which may account for the modest level of Arf4 depletion. In Arf1+Arf4 depleted cells, BACE1-GFP accumulated in the TGN, as expected, but to a lesser extent than single depletion of Arf4 (Fig. 8B & C). Quantitation revealed an increase in BACE1-GFP co-localization with golgin-97 from 8% in control cells to 17.1 $\pm$ 4.8% in Arf1+Arf4 depleted cells (Fig. 8D). These data show that the double depletion of Arf1 and Arf4 did not result in a further increase in the level of BACE1-GFP in the TGN compared with single knockdowns, indicating that Arf1 and Arf4 are unlikely to have overlapping functions in regulating the export of BACE1 from the TGN.

To investigate whether AP-1γ, Arf1 and Arf4 also are required for the Golgi export of APP, AP-1γ, Arf1, and Arf4 were depleted in HeLa cells stably expressing APP_{695wt} (HeLa-APP_{695wt}); this cell line has been previously described (Toh *et al.*, 2017). None of these knockdowns altered the localization of APP at the TGN compared to cells treated with control siRNA as shown by quantitative analyses (Fig. S5). These data indicate that the AP-1/Arf1/Arf4 sorting machinery is not required for APP export from the TGN.

Depletion of either AP-1, Arf1, or Arf4 reduces the cell surface expression of BACE1

As depletion of AP-1, Arf1 and Arf4 resulted in the accumulation of BACE1 in the TGN, we quantified their effect on the cell surface levels of BACE1 by flow cytometry. AP-1γ depleted HeLa-BACE1-GFP cells showed a reduction of cell surface BACE1 compared with control conditions (Fig. 9A). There was a decrease of BACE1 mean fluorescence intensity of 19.8% in AP-1γ depleted cells compared to control siRNA-treated cells (Fig. 9D) whereas cell surface expression of BACE1 was unaltered in either AP-4ε or Arl5b depleted cells (Fig. 9B & E). Therefore, the cell surface levels of BACE1 is dependent on AP-1 mediated trafficking of BACE1 from the Golgi.

The impact of Arf1 and Arf4 depletion on the cell surface levels of BACE1 was also examined. The depletion of either Arf1 or Arf4 in HeLa-BACE1-GFP resulted in a decrease in cell surface expression of BACE1, as shown by a leftward shift in the fluorescence intensity peaks of each knockdown condition compared to control conditions (Fig. 9C). Quantitative analysis showed a very similar decrease in BACE1 mean fluorescence intensity by 36.3% and 39.3% in cells treated with either Arf1 siRNA or Arf4 siRNA, respectively, compared to control conditions (Fig. 9F). The decrease in cell surface expression of BACE1 demonstrates that Arf1 and Arf4 are also required for the trafficking of BACE1 to the cell surface. Taken together these results show that cell surface expression of BACE1 is dependent on the Golgi AP-1 export pathway.

The trafficking of transferrin receptor to the cell surface is independent of the AP-1/Arf1/Arf4 pathway

The question arises whether the AP-1 pathway to the cell surface is used by other cargoes. AP-1 has been shown to be required for the trafficking of transferrin receptor (TfR) to the basolateral PM in polarized Madin-Darby Canine Kidney (MDCK) epithelial cells (Gravotta *et al.*, 2012) and the trafficking of TfR to the somatodendritic PM in rat hippocampal neurons (Farias *et al.*, 2012). Therefore, we assessed whether the trafficking of TfR to the cell surface in non-polarized HeLa cells is also AP1-dependent. The cell surface expression of TfR in AP-1 depleted HeLa-BACE1-GFP was assessed by flow cytometry. Surprisingly, the depletion of AP-1γ showed no significant change in the level of cell surface TfR compared with control cells (Fig. S6 A & C). We also assessed the cell surface expression of TfR in either Arf1 or Arf4 depleted cells. The depletion of Arf1 showed no change and Arf4 a minor increase in the level of cell surface TfR, compared with control cells (Fig. S6 B & D). These findings demonstrate that AP-1, Arf1, and Arf4 are not required for the trafficking of all membrane cargo to the PM; rather these machineries are likely to be required for a subset of cargo, which includes BACE1, from the TGN to the PM.

Impact of delayed trafficking of newly synthesized BACE1 from the TGN on amyloidogenic processing of APP

To assess whether the accumulation of BACE1 at the TGN following AP-1, Arf1, and Arf4 depletion alters amyloidogenic processing of APP, we analyzed the processing of APP by endogenous BACE1 and γ-secretase in HeLa-APP_{695wt} cells. Conditioned medium from siRNA-treated HeLa-APP_{695wt} cells was collected and analyzed for secreted Aβ using a sandwich ELISA specific for human $Aβ_{40}$. The $Aβ_{40}$ levels were normalized to total cellular protein for each sample. There was a 1.7-fold increase in secreted Aβ from AP-1γ depleted cells compared to control cells (Fig. 10A). In addition, there were 2.7-fold, 4.5-fold, and 3.5-fold increase in secreted Aβ from Arf1, Arf4, and Arf1+4 depleted conditions, respectively, compared with control conditions (Fig. 10B). The increase in Aβ production indicates enhanced processing of APP by endogenous BACE1 at the TGN following the depletion of AP-1, Arf1, and Arf4 sorting machinery. A higher level of secreted Aβ was detected from Arf4 depleted cells than Arf1 depleted cells (Fig. 10B), consistent with the finding that BACE1 showed a greater accumulation at the TGN in Arf4 depleted cells (Fig. 8B & D).

To directly assess the level of β-CTF/C99 derived from the initial cleavage of APP by BACE1, cell extracts were probed with the W0-2 antibody, which recognises residues 4-10 of the Aβ domain in APP and which will detect full length APP and β-CTF/C99. Full-length APP was detected in HeLa-APP_{695wt} cell extracts (Fig. S7), whereas in the absence of the γ-secretase inhibitor, DAPT, β-CTF/C99 was not detected in control siRNA-treated cells and only detected at low levels in cells treated with AP-1γ siRNA even after long exposures (Fig. 10C, Fig S7A). However, in the presence of DAPT, β-CTF/C99 was readily detected in both control siRNA- and AP-1γ siRNA- treated samples. Moreover, there was a 2.8-fold increase in the level of intracellular β-CTF/C99 in AP-1γ depleted conditions compared with control conditions (Fig. 10C & E). In Arf1 siRNA, Arf4 siRNA, or Arf1+4 siRNAs depleted conditions, β-CTF/C99 was again detected only at low levels in the absence of DAPT (Fig. 10D). In the presence of DAPT, there was also a 2.7-fold, 3.9-fold, and 4.1-fold increase in the level of intracellular β-CTF/C99 detected in cells treated with either Arf1 siRNA, Arf4 siRNA, or Arf1+4 siRNAs, respectively, compared with control siRNA-treated cells (Fig. 10 D & E). The increase in β-CTF/C99 production directly demonstrates that the depletion of AP1γ, Arf1, Arf4, or Arf1+4 enhances BACE1 cleavage of APP at the TGN. Notably, a greater increase in the level of β-CTF/C99 was detected in Arf4 depleted condition than in Arf1 depleted condition (Fig. 10D & E), consistent with the level of Aβ production in these knockdown

conditions (Fig. 10B). The similar increase in β-CTF/C99 detected in both Arf4 and Arf1+Arf4 knockdown conditions is likely due to more efficient depletion of Arf4 (>80%) in this experiment (Fig. 10D) compared to the previous experiment (Fig. 8A). These results again indicate that Arf4 is likely to be the major small G protein regulating the post-Golgi trafficking of BACE1. Collectively, these findings highlight the relevance of AP-1, Arf1, and Arf4 trafficking machinery on the regulation of the amyloidogenic processing of APP at the TGN.

Depletion of AP-1 in neurons resulted in enhanced BACE1 processing of endogenous APP

Next, we assessed whether APP processing by endogenous BACE1 in the TGN of primary neurons is also regulated by the AP-1 pathway. As residues 4-10 of the Aβ domain in APP, detected by W0-2 antibody, differs between human and mouse, the W0-2 antibody is not suitable for the detection of β-CTF/C99 in primary mouse cortical neurons. Instead, we employed the Y188 antibody, which was raised against the highly conserved YENPTY sorting motif of APP (residues 682-687 of APP695). The Y188 antibody detects both β-CTF/C99 (11 kDa) and α-CTF/C83 (9 kDa) in primary mouse cortical neurons (Tan and Gleeson, 2019c).

We utilised two different shRNA targets to AP-1 for the generation of recombinant lentivirus to deplete AP-1 in primary mouse cortical neurons. The depletion of AP-1 in population of transduced neurons was then assessed by immunoblotting. AP-1γ was depleted by 43–46% in neurons transduced with AP-1γ-shRNA1 and AP-1γ-shRNA2 lentivirus when compared to non-transduced neurons (Fig. 11A & B). Based on GFP-positive neurons, the transduction efficiency of the transduced neuronal population was 35-50%, indicating that the depletion of AP-1 in GFP-positive neurons was ~90%. In the absence of DAPT, β-CTF/C99 and α-CTF/C83 were not detected in any of the neuronal extracts (Fig. 11A), consistent with previous findings (Tan and Gleeson, 2019c) and indicating that the products of α- and β-secretase cleavage are rapidly processed by γ-secretase. However, in the presence of DAPT, there were a 1.88- and 1.94- fold increase in the level of intracellular β-CTF/C99 in neurons transduced with AP-1γ-shRNA1 and AP-1γ- shRNA2, respectively, compared with non-transduced neurons (Fig. 11A & C). We treated AP-1γ-shRNA1 and AP-1γ-shRNA2 transduced neurons with a BACE1 inhibitor C3 to validate that the increased in the 11 kDa band (β-CTF/C99) was specifically due to enhance cleavage of APP by BACE1. In the presence of C3 and DAPT, the 11 kDa band (indicated by *) were absent (Fig. 11A), confirming their identity as β-CTF/C99. Moreover, there were no significant changes in the level of α-CTF/C83 (** band) in AP-1γ-shRNA1 and AP-1γ-shRNA2 transduced neurons

compared to non-transduced neurons (Fig. 11A & D). Full length APP was also detected in these immunoblots (Fig. S7B shows the entire blot). Collectively, AP-1 depletion results in an increased level of β-CTF/C99, but not α-CTF/C83, demonstrating that AP-1 depletion enhances amyloidogenic processing of APP by BACE1.

Processing of APP by BACE1 and γ-secretase in neurons results in the production of the two major species of amyloid peptides, Aβ40 and the more highly cytotoxic Aβ42. To determine the levels of Aβ40 and Aβ42 exported into the cell medium of treated neurons, conditioned medium from shRNA-treated neurons was collected and analyzed for secreted Aβ40 (Fig. 11E) and Aβ42 (Fig. 11F) using mouse Aβ40 and Aβ42 specific ELISAs. We confirmed that these Aβ-ELISAs were specific for the individual Aβ peptides (not shown). In non-transduced neurons the ratio of secreted Aβ40 :Aβ42 was 5.3:1, consistent with Aβ40 representing the major species from neuronal tissues (Schieb *et al.*, 2011). In AP-1 silenced neurons, there was an increase in levels of both Aβ species, for $A\beta_{40}$ there was a 3.0-fold increase and for Aβ42 a 3.7-fold increase. Therefore, the Golgi associated APP processing events in primary neurons results in the generation of the cytotoxic Aβ42 species.

Discussion

There is considerable evidence from GWAS analysis and experimental animal models that dysfunctional membrane trafficking contributes to aberrant Aβ production and AD. Many studies have also indicated that Aβ can be generated in both the endosomal and secretory pathway (Tan and Gleeson, 2019b). We and others have shown that the TGN is a major site for Aβ production along the secretory pathway (Burgos *et al.*, 2010; Toh *et al.*, 2017). As newly synthesized APP and BACE1 are co-transported along the secretory pathway it is important to understand how the trafficking of these two membrane cargos are regulated to control the cleavage of APP by BACE1. We previously showed that newly synthesised APP is transported from the TGN directly to the early endosomes by an AP-4 dependent pathway. Here we have examined the sorting and trafficking of newly synthesized BACE1 at the Golgi in both HeLa and primary neurons and have shown that (1) newly synthesized BACE1 traffics from the TGN to the PM; (2) the AP complex, AP-1, and Arf1 and Arf4 small G proteins are essential for TGN-to-PM trafficking of BACE1; (3) the post-Golgi trafficking of APP is independent of the AP-1/Arf1/Arf4 regulated pathway; (4) the depletion of either AP-1, Arf1, or Arf4 enhanced the amyloidogenic processing of APP and (5) in primary neurons the depletion of AP-1 increased the levels of both secreted $A\beta_{40}$ and $A\beta_{42}$, demonstrating that the cytotoxic $A\beta_{42}$ can be generated in the secretory pathway. Collectively, our

findings indicate that the AP-1/Arf1/Arf4 dependent transport pathway is crucial for the efficient export of BACE1 from the Golgi to the PM, which in turn limits the processing of APP at the TGN.

We used the RUSH-system to track the anterograde itinerary of newly synthesized BACE1 (BACE1-SBP-GFP) as it provides an effective approach to synchronize protein trafficking along the anterograde pathway (Boncompain *et al.*, 2012; Chen *et al.*, 2017). BACE1-SBP-GFP was transported to the Golgi within 10-15 min following release from the ER by addition of biotin, and then trafficked from the TGN to the PM. Our data strongly indicates that BACE1 is transported directly from the TGN to the PM. This conclusion is based on quantitative analysis of confocal live imaging, TIRF analysis, and fast image acquisition which showed that BACE1-SBP-GFP-containing vesicles were transported from a juxtanuclear compartment directly to the distal edge of the cell. Also, given that BACE1 was detected arriving at the plasma membrane 20 min after addition of biotin whereas it was first detected in recycling endosomes at a later time point (30 min), implies a direct Golgi-to-PM transport step. Arrival of BACE1 at the early and recycling endosomes at the 30 min time point and most likely represents internalized BACE1 from the PM (Chia *et al.*, 2013). The intracellular distribution of BACE1-SBP-GFP at an extended time point was very similar to the steady state distribution of BACE1 in either stable of transiently transfected HeLa cells, with or without a GFP tag (Chia *et al.*, 2013), indicating that the SBP and GFP tags are unlikely to interfere with the trafficking of BACE1-SBP-GFP in the RUSH system.

The current studies involved silencing of trafficking machinery in a stable cell line expressing only modest levels of BACE1-GFP, to minimize the possibility of saturation of the post-Golgi transport machinery (Chia *et al.*, 2013). The physiologically relevance of our studies in HeLa cells was confirmed by the demonstration that endogenous BACE1 in neurons was found mainly in the recycling endosomes and early endosome under steady state conditions, with minor levels in the Golgi and late endosomes/lysosomes, a distribution similar to transfected HeLa cells; and by the observation that silencing AP-1, but not AP-4, in neurons resulted in the accumulation of endogenous BACE1 in the TGN. Confirmation of the findings in HeLa cells with the behaviour of endogenous BACE1 in primary neurons demonstrates that the post-Golgi transport pathways of BACE1 are common between the cell types.

A key finding of this work is that AP-1 is required for the efficient post-Golgi sorting of BACE1 in both HeLa cells and neurons. BACE1 was retained in the Golgi/TGN following AP-1 knockdown, as revealed by localisation studies of fixed cells with defined markers and by the analysis of the kinetics of BACE1 transport through the Golgi in live cells using RUSH. In addition,

the reduced levels of BACE1 at the cell surface in AP-1 knockdown cells, as assessed by FACS of non-permeabilized cells, is also consistent with the retention of BACE1 in the Golgi. In contrast, GGA1, which is also found at the Golgi, is not required for the post-Golgi export of BACE1. Rather GGA1, which can interact with a DISLL motif in the cytoplasmic tail of BACE1, is required for the endosomal sorting of BACE1 (He *et al.*, 2002; He *et al.*, 2005; Toh *et al.*, 2018). Interestingly, the DISLL motif is part of an acidic cluster (DDFADDISLL) motif in the cytoplasmic tail BACE1 that has similar properties to other acidic cluster sequences in proteins which are known to associate with AP-1 (Table 2). The basic patch (Lys274, Lys298, Lys302, Arg303, and Arg304) of the AP-1μ subunit has been shown to be required for the binding of acidic cluster sequences (Navarro Negredo *et al.*, 2017). Based on the findings in this paper, AP-1 is likely to interact with BACE1 via the acidic motif at the TGN and recruit this membrane cargo into a transport pathway that directs BACE1 to the PM. A previous study analyzing the AP-2-mediated endocytosis of BACE1 mutated D495 in the acidic cluster motif (DDFAD$_{495}$DISLL) in BACE1 to R495 (Prabhu *et al.*, 2012). These authors showed that the D495 residue is essential for AP-2-mediated endocytosis of BACE1 (Prabhu *et al.*, 2012). However, an additional effect of the D495R mutation, which was not alluded to by these authors, was the accumulation of D495R BACE1 mutant in the juxtanuclear region of the cell (Prabhu *et al.*, 2012), suggesting that the acidic D495 residue could also be important for the post-Golgi trafficking of BACE1. Direct evidence that AP-1μ interacts with the acidic cluster motif of BACE1 remains to be formally shown.

The recruitment of AP-1 to the TGN is known to be mediated by Arf1 and Arf4 small G proteins (Stamnes and Rothman, 1993; Lee *et al.*, 2008; Nakai *et al.*, 2013) and we have shown that both these small G proteins are also required for the sorting of BACE1 at the Golgi. The depletion of either Arf1 or Arf4 resulted in the accumulation of BACE1-GFP in the TGN. In contrast to BACE1, the depletion of either AP-1, Arf1 or Arf4 did not affect the distribution of APP. We have previously shown that depletion of Arf1 or Arf4 does not affect recruitment of AP-4 to the TGN (Toh *et al.*, 2017). These findings further support the conclusion that the post-Golgi sorting machinery and trafficking pathways that regulate APP and BACE1 differ.

Depletion of AP-1, Arf1, or Arf4, resulted in a reduction of BACE1 at the cell surface. Nonetheless, substantial levels of BACE1 were present at the surface in these depleted cells which could be due to either the incomplete knockdown of the transport machinery or transport by an AP-1 independent mechanism. On the other hand, depletion of either AP-1, Arf1, or Arf4 did not reduce the level of TfR at the cell surface, consistent with the findings from the Bonifacino laboratory which showed that TfR is loaded into tubular carriers derived from the TGN in non-

polarised HeLa cells by an AP-1 independent process (Chen *et al.*, 2017). Thus, it is clear there are multiple transport pathways to the PM and the AP-1 pathway may be selective for a subset of membrane cargoes which includes BACE1.

AP-1 has been reported to facilitate membrane cargo trafficking along a number of transport pathways. Although not generally considered to be a cargo adaptor for transport to the PM, a previous study of a reovirus membrane protein also reported the transport to the plasma membrane from the Golgi by a AP-1 dependent pathway (Parmar and Duncan, 2016). AP-1B, which is a distinct isoform of AP-1 bearing a μ1B subunit, is important for transport of cargo from the recycling endosomes to the PM in a subset of polarized epithelial cells, however, AP-1B is absent in non-epithelial cells (see (Tan and Gleeson, 2019a)). AP-1 is known to regulate the TGN to endosomal pathway required for the delivery of newly synthesized lysosomal enzymes bound to mannose 6-phosphate receptors (MPRs) from the TGN to the late endosomes (Hille-Rehfeld, 1995; Meyer *et al.*, 2000). A key question arising from our study is how AP-1 regulates the trafficking of cargoes from the TGN to the PM as well as the TGN to late endosomes. The GGA proteins, which are also recruited to the TGN by Arf1, have been shown to function cooperatively with AP-1 to regulate the trafficking of cargoes from the TGN to the endosomes (Doray *et al.*, 2002; Hirst *et al.*, 2012). These studies suggest that the combination of AP-1 and GGA is likely to regulate the sorting of cargoes to the endosomes from the TGN. On the other hand, GGAs are not required for the trafficking of BACE1 to the PM. Therefore, cargo which interacts selectively with AP-1 at the TGN may be transported from the Golgi directly to the PM. In addition to these anterograde pathways, AP-1 has also been reported to regulate retrograde transport in the Golgi in yeast cells (Casler et al, 2019).

An important component of the current study was to determine the consequence of retention of BACE1 in the Golgi on APP processing. Using stably transfected HeLa-APP_{695wt} cells, we showed that Golgi export of endogenous BACE1 by the AP-1 pathway is essential for the regulation of amyloidogenic processing. Upon the depletion of either AP-1, Arf1, or Arf4, there was increased processing of APP as demonstrated by a 2.8-4.1-fold increase of intracellular β-CTF/C99 and a 1.7-4.5-fold, increase in secreted Aβ secretion compared with control conditions. Moreover, AP-1 depletion in primary neurons resulted in 1.9-fold increase in the level of intracellular β-CTF/C99 and 3.1 and 3.7-fold increase in secreted $Aβ_{40}$ and $Aβ_{42}$, respectively. These findings demonstrate that the AP-1 pathway is critical for regulating processing events under physiological conditions. In addition, although $Aβ_{40}$ was the predominant species in neurons, as expected from previous reports (Schieb *et al.*, 2011), the finding that $Aβ_{42}$ is generated via TGN-

mediated processing of APP is an important observation as $A\beta_{42}$ is more cytotoxic than $A\beta_{40}$ (Lane *et al.*, 2017) and has not, to our knowledge, been previously demonstrated to be produced from APP processing events within the secretory pathway.

The trafficking of BACE1 to the PM via the AP-1 pathway may serve as a regulatory mechanism to segregate BACE1 from APP at the TGN, thus limiting the amyloidogenic processing of APP in this compartment. This conclusion is also consistent with our earlier study where enhanced APP cleavage was detected at the TGN upon the redirection of BACE1 recycling to this compartment using a BACE1/TGN38 chimera (Chia *et al.*, 2013). Only low levels of β-CTF/C99 were detectable in AP-1/Arf1/Arf4 depleted cells in the absence of the γ-secretase inhibitor, indicating that γ-secretase rapidly processes β-CTF/C99. Given that γ-secretase is also localized in the Golgi compartment (Rechards *et al.*, 2003), the liberation of Aβ peptide from β-CTF/C99 by γ-secretase is also likely to occur in the TGN. The secretion of Aβ peptide from the cell is proposed to occur through various anterograde trafficking pathways [reviewed in (Toh and Gleeson, 2016)]. We propose that the loss of the AP-1/Arf1/Arf4 transport machinery results in the accumulation of BACE1 in the TGN, which results in a loss in the segregation of BACE1 from newly synthesized APP arriving at the TGN (See Fig. 11G). The increase in convergence between BACE1 and APP in the TGN then leads to increased processing of APP by BACE1 in this compartment.

In conclusion, a functional AP-1/Arf1/Arf4 pathway is required for the export of BACE1 from the Golgi directly to the PM. On the other hand, the trafficking of APP from the TGN is independent of this pathway. Rather, the trafficking of APP from the TGN is regulated by the AP-4/Arl5b transport machinery directly to the endosomal pathway. The anterograde pathways for BACE1 and APP are illustrated in Fig. 11G. The requirement for distinct transport machinery for post-Golgi transport of APP and BACE1 provides a mechanism to sort and segregate APP and BACE1 into separate pathways. Therefore, the convergence between APP and BACE1 along the anterograde pathway would be limited, which in turn would minimize the extent of amyloidogenic APP processing and Aβ production.

Experimental procedures

Plasmids and antibodies

Streptavidin fused to the ER retention signal Ii (human major histocompatibility complex class II invariant chain), and full-length wild-type BACE1 fused with a streptavidin-binding peptide (SBP) and EGFP-tag were inserted into pIRESneo3 (Str-Ii_BACE1FL-SBP-EGFP). Constructs encoding human wild-type Arf1 and Arf4 tagged with mCherry at their C-termini, pcDNA3/hArf1(WT)-mCherry (Addgene plasmid: #79419) and pCAG/hArf4(WT)-mCherry (Addgene plasmid: #79406), respectively, were gifts from Kazuhisa Nakayama. pGIPZ-shRNA lentiviral constructs against mouse AP-1γ (V2LMM_44992 and V3LMM_442644) were purchased from Dharmacon, GE Healthcare. pGIPZ-shRNA lentiviral constructs against mouse AP-4ε, pCMV-VSV-G and psPAX2 were previously described (Tan and Gleeson, 2019c).

Rat monoclonal antibodies to mouse LAMP1 (Clone 1D4B, #553792), mouse monoclonal antibodies to AP-1γ (Clone 88, #610385), AP-4ε (Clone 32, #612019), EEA1 (Clone 14, #610456), Rab4 (Clone 7, #610889) and Rab11 (Clone 47, #610656) were purchased from BD Biosciences. Mouse monoclonal antibodies to human golgin-97 (CDF4, #A21270) was purchased from Thermo Fisher Scientific. Mouse monoclonal antibodies to human CD63 (MX-49.129.5, #sc-5275) were purchased from Santa Cruz Biotechnology. Mouse monoclonal antibodies to $A\beta_{4\text{-}10}$ (W0-2, #MABN10) was from Merckmillipore (MERCK, USA). Rabbit monoclonal antibodies to GGA1 (#ab170956) and APP (Clone Y188, #ab32136), and mouse monoclonal antibodies to Arf1 (ARFS3F1, #ab11038) were obtained from Abcam (Cambridge, UK). Rabbit monoclonal antibodies to β-secretase (BACE1) (D10E5, #5606) was from Cell Signaling Technology. Rabbit polyclonal antibodies to BACE1 (N-terminus 46–62, Clone EE17, #B0681), mouse monoclonal antibodies to APP (Clone NAB228) and mouse monoclonal antibodies to α-tubulin (Clone DM1A, #T9026) were bought from Sigma-Aldrich (MERCK, USA). Rabbit polyclonal anti-GCC88 antibodies (Luke *et al.*, 2003) and human autoantibodies to p230/golgin-245 (Kooy *et al.*, 1992) have been described. Rabbit polyclonal antibodies to Arf4 (#11673-1-AP) were from ProteinTech. Mouse monoclonal antibodies to human transferrin receptor (TfR/OKT9) (Schneider *et al.*, 1982) were purified from supernatants from a hybridoma. Can Get Signal® Immunoreaction Enhancer Solution (Toyobo Life Science, Japan) was used to dilute mouse anti-Rab11 antibodies for immunofluorescence analysis.

Goat anti-mouse IgG-Alexa Fluor 488 nm, goat anti-mouse IgG-Alexa Fluor 568

nm, goat anti-mouse IgG-Alexa Fluor 647 nm, goat anti-rabbit IgG-Alexa Fluor 488 nm, goat anti-rabbit IgG-Alexa Fluor 568 nm, goat anti-rabbit IgG-Alexa Fluor 647 nm, goat anti-rat IgG-Alexa Fluor 568 nm, and goat anti-human IgG-Alexa Fluor 647 nm (for human anti-p230/golgin-245 antibodies) conjugated secondary antibodies for immunofluorescence were obtained from Thermo Fisher Scientific. Horseradish peroxidase (HRP)-conjugated rabbit anti-mouse Ig and HRP-conjugated swine anti-rabbit Ig were bought from DAKO Corporation (CA, USA).

RNAi and transient transfections

The silencing of AP-1 γ-adaptin, AP-4 ε-adaptin, GGA1, Arl5b, Arf1 and Arf4 was conducted using short-interfering RNA (siRNA) duplexes manufactured by Sigma-Proligo (Australia). Cell monolayers were transfected with siRNA using DharmaFECT1 (Thermo Fisher Scientific) according to manufacturer's protocol and incubated for 72 h in a humidified 10% CO_2 incubator at 37^0C. AP-1γ siRNA (Camus *et al.*, 2007), GGA1 siRNA (Toh *et al.*, 2018), Arl5b siRNA (Houghton *et al.*, 2012), Arf1 siRNA (Southon *et al.*, 2011), AP-4ε siRNA and Arf4 siRNA (Toh *et al.*, 2017) have been previously described.

Transient transfection of Arf1-mCherry and Arf4-mCherry plasmids were conducted for 24 h using FuGENE® 6 (Promega, USA) as per manufacturer's protocol.

Generation of HeLa cells stably expressing BACE1-GFP (HeLa-BACE1-GFP)

Parental HeLa cells were transfected with the pBACE1-EGFP-N3 construct using FuGENE® 6 (Promega,USA). Stably expressing cells were selected in C-DMEM supplemented with 1.5 mg/mL G418 for two weeks. The resultant polyclonal HeLa-BACE1-GFP cells were harvested and GFP-positive cells were single-cell sorted into 96-well plates using a BD Influx™ cell sorter (BD Bioscience) at the Murdoch Children Research Institute (MCRI), Victoria, Australia. HeLa-BACE1-GFP stable clones were validated by immunofluorescence, immunoblotting, and flow cytometry. Cells were maintained in C-DMEM supplemented with 1 mg/mL G418 and cultured in a humidified 10% CO_2 incubator at 37^0C.

Cell culture

Authentic and mycoplasma-tested HeLa cells (Scherer *et al.*, 1953) were maintained as semi-confluent monolayers in Dulbecco's modified Eagle's medium (DMEM) (Thermo Fisher Scientific, Australia) supplemented with 10% v/v foetal calf serum (FCS) (Gibco®, Thermo Fisher Scientific), 2 mM L-glutamine, 100 units/μL penicillin and 0.1% w/v streptomycin (complete DMEM/C-DMEM). HeLa-APP_{695wt} cell line was generated as previously described (Toh *et al.*, 2017) and maintained in C-DMEM supplemented with 500 ng/mL puromycin (Invitrogen, Thermo Fisher

Scientific). HEK293T packaging cells were maintained as semi-confluent monolayers in C-DMEM without penicillin and streptomycin (C-DMEM –P/S). All cells were cultured in a humidified 10% CO_2 incubator at 37^0C.

Primary mouse cortical neuronal cultures

All experiments carried out on animals (Ethics ID: 1613960) were in accordance with animal ethics guidelines (approval number: 1212502.1) approved by the Animal ethics committee, The University of Melbourne. Primary cortical neurons were prepared from the collected embryos of a pregnant mice (C57BL/6) at gestational day 15-16 and cultured as previously described (Tan and Gleeson, 2019c). Primary cortical neurons were plated at a density of 1.2 x 10^5 cells/well (12-well plates) and 5 x 10^5 cells/well (6-well plates), and cultured in neurobasal medium supplemented with 2.5% B-27, 0.25% GlutaMAX and 100 units/μL penicillin and 0.1% streptomycin (complete NBM) (Life Technologies, USA).

Generation of lentivirus and transduction of primary mouse cortical neuronal cultures

Recombinant lentiviruses were generated and used for transduction of primary mouse cortical neurons as previously described (Tan and Gleeson, 2019c). Briefly, lentivirus was generated via calcium phosphate transfection of the HEK293T packaging cells with lentiviral plasmids at a ratio of 7 pCMV-VSV-G : 3 psPAX2 : 10 pGIPZ-shRNA. Cells were transfected overnight in a humidified 10% CO_2 incubator at 37^0C. The existing medium was then replaced with fresh medium and cells were incubated for a further 48 h to allow the production of viral particles. Virus-containing medium was harvested, centrifuged to pellet cell debris, and the viral supernatant filtered using Steriflip-HV sterile centrifuge tube top filter unit (MERCK). PEG-it virus precipitation solution (Integrated Sciences, Australia) was added to the filtered viral medium at 1x final and incubated overnight at 4^0C. Viral particles were pelleted by centrifugation and resuspended in DMEM/NBM supplemented with 10 mM HEPES (Gibco®, Thermo Fisher Scientific) at 1:100 of its original harvested volume. Concentrated virus was allocated into cryovials, snap freeze on dry ice, and stored at -80^0C.

Primary mouse cortical neurons were transduced at day 3 in vitro (DIV 3) with 10–15 μL/well (12-well plate) of either AP-1γ-shRNA or AP-4ε-shRNA lentivirus diluted with fresh C-NBM to a final volume of 200 μL/well. Transduced neurons were incubated for 24 h (DIV 4) in a 37^0C incubator with 10% CO_2, followed by replacement of lentiviral medium with conditioned C-NBM (half fresh C-NBM and half C-NBM recovered from neuronal culture) and incubated for a further 72 h (DIV 7).

Immunofluorescence analyses

Monolayers of cultured mammalian cells and primary mouse cortical neurons were fixed in 4% paraformaldehyde (PFA; Wako Pure Chemical Industries, Japan) for 15 min at room temperature (RT), quenched in 50 mM NH_4Cl/PBS for 10 min at RT, permeabilized with 0.1% v/v Triton X-100/PBS for 4 min at RT, and blocked in blocking solution (5% v/v FCS and 0.02% v/v sodium azide, in PBS) for 30 min to reduce non-specific binding. All staining was conducted using the above method except for mouse anti-Rab11, anti-Rab4 and mouse anti-AP1γ antibodies. For Rab11 staining, cells were fixed with 10% trichloroacetic acid (TCA) on ice for 15 min, quenched in 30 mM glycine/PBS for 10 min at RT, then permeabilized and blocked as above. For AP-1γ staining, cells were fixed in 4% PFA for 15 min, quenched in 50 mM NH_4Cl/PBS for 10 min, permeabilized in 0.1% v/v Triton X-100/PBS for 15 min, then blocked with 1% w/v BSA/0.3% v/v Triton X-100/PBS for 1 h. To stain for Rab-4 in neurons, cells were fixed in cold 100% Methanol and incubated at -20^{0}C for 5 min and blocked as above. Cultured cells were stained with primary antibodies diluted in blocking solution, with the exception where mouse anti-Rab11 antibodies were diluted in Can Get Signal® Immuno-reaction Enhancer Solution (Toyobo Life Science, Japan), for 1 h at RT. Staining of neurons with primary antibodies were conducted overnight at 4^{0}C. Cultured cells and neurons were washed with PBS and stained with fluorophore-conjugated secondary antibodies diluted in blocking solution for 30 min at RT. Coverslips were washed with PBS then distilled water and mounted in Mowiol (10% w/v Hopval 5-88, 25% w/v glycerol, 0.1 M Tris in milli-Q water) on microscope glass slide. For staining the TGN in HeLa cells, mouse anti-golgin-97 was routinely used, with the exception where primary antibodies to Rab11, EEA1 and APP were used in which case rabbit anti-GCC88 was used instead. As mouse anti-golgin-97 and rabbit anti-GCC88 antibodies are specific for their respective human antigens, and do not cross-react with the mouse homologues, human autoantibodies to p230/golgin-245 were used for TGN staining in primary mouse cortical neurons.

Images were acquired sequentially for multi-colour imaging on a laser confocal scanning microscope (Leica TCS SP8 confocal imaging system) using a 63X 1.4 NA HCX PL APO CS oil immersion objective and a Leica HyD photodetector. GFP and Alexa Fluor 488 were excited using the 488 nm line source of an Argon laser. Alexa Fluor 568 and Alexa Fluor 647 were excited with the 543 nm and 633 nm Helium-neon (HeNe) laser, respectively. DAPI was excited with a 405 nm UV laser. Images for HeLa cells were acquired at 0.3 μm single section and images for primary neurons were acquired as Z-stacks of 5-6 sections at 0.2 μm per section.

Anterograde transport assay of BACE1 using the RUSH system

HeLa cells were cultured as monolayers in 12-well or 24-well and were transfected with calcium phosphate (Jordan et al, 1996). Transfected cells were incubated for 24 h at 37^0C with 10% CO_2. D-biotin (Sigma-Aldrich, MERCK) at 40 μM final concentration was added to transfected cells to allow the synchronous release of BACE1-SBP-GFP from the streptavidin-Ii hook protein in the ER.

For live imaging, an inverted Nikon Eclipse Ti microscope (with optical autofocus system and a motorized piezo stage) was used with a 100X oil-immersed objective. Round (24 mm) coverslips with HeLa cell monolayers were clipped in a metal chamber, maintained in Leibovitz's medium (Thermo-Fisher Scientific) and incubated at 37°C during the imaging. Images with z-stacks (11 steps, step size 0.4 μm) were captured every 1 or 2 min for 60 min after addition of 40 μM D-biotin to the medium with an Andor Ixon Ultra (EM-CCD) camera and using Metamorph software (Molecular devices). Laser power and acquisition settings were chosen to avoid photobleaching and settings were identical for control and siRNA treated samples. For fast acquisition, images were collected in real time every 2 sec. Temporal projections (Fig. 2B) were performed with the tool "temporal-color-code" on the Fiji software for the entire movie (15 min of biotin to 45 min biotin 1 to 601).

TIRF experiments were performed using the same device. Images were collected every 10 sec from time point 1 to time point 170 and then every 2 sec until the end.

Flow cytometry for cell surface expression analyses

Control, AP1γ, AP4ε, Arl5b, Arf1, or Arf4 depleted HeLa-BACE1-GFP cells were lifted from a 6-well plate with 5 mM EDTA/PBS at 37^0C. Live cells were stained in suspension with either rabbit anti-BACE1 (EE17) antibodies or mouse anti-TfR/OKT9 antibodies for 30 min on ice. Cells were washed twice with ice-cold PBS, fixed with 4% PFA for 15 min at RT, quenched with 50 mM NH_4Cl for 10 min at RT, and blocked for 30 min at RT. To detect antibody-bound complexes, cells were incubated with Alexa Fluor conjugated secondary antibodies for 30 min. Cells were washed with PBS and resuspended in 2 mM EDTA/PBS. Cells were analyzed by medium flow rate in a BD LSRFortessa flow cytometry (BD Biosciences) and 10, 000 events were collected with a forward scatter threshold of 5000. Data were analyzed using FlowJo V10.

Aβ ELISAs

Aβ40-specific human ELISA (enzyme-linked immunosorbent assay) (#KHB3481), Aβ40-specific mouse ELISA (#KMB3481) and Aβ42-specific mouse ELISA (#KMB3441) kits were purchased

from Invitrogen, Thermo-Fisher Scientific. Aβ ELISA kits were used to measure either secreted human Aβ40 levels in 16 h conditioned medium, or secreted mouse Aβ40 and Aβ42 levels in 20 h conditioned medium following the manufacturer's protocol. Levels of secreted Aβ were normalized to total cellular protein concentrations measured by Bradford assay.

γ-secretase inhibitor (DAPT) and BACE1 inhibitor (C3) treatment

HeLa cell monolayers were treated with either 0.01% v/v DMSO (carrier control) or 250 nM γ-secretase inhibitor N-[N-(3,5-difluorophenacetyl)-l-alanyl]-S-phenylglycine t-butyl ester (DAPT) (Sigma-Aldrich, MERCK, USA). Primary mouse cortical neurons were treated with either 0.01% v/v DMSO (carrier control), 2 μM DAPT or 2 μM β-secretase/BACE1 inhibitor C3 (Calbiochem, MERCK, USA). HeLa cells and neurons were incubated for 16 h and 20 h, respectively, in a 37^0C incubator with 10% CO_2.

Cell extracts for immunoblotting

Cellular lysates were extracted using radioimmunoprecipitation (RIPA) lysis buffer (50 mM Tris-HCl, pH 7.3, 150 mM NaCl, 0.1 mM EDTA, 1% w/v sodium deoxycholate, 1% v/v Triton X-100, 0.2% w/v NaF, and 100 μM Na_3VO_4) supplemented with 1X cOmplete^{TM} Mini Protease Inhibitor Mixture (Roche Applied Science, Sigma, and Merck). Cell lysates were incubated 10 min on ice followed by centrifugation at 16,000 xg at 4°C for 10 min. Protein concentration was determined by the Bradford protein assay (Bio-Rad) using bovine serum albumin (BSA) protein standards (Pierce BSA standard, Thermo-Fisher Scientific).

β-CTF/C99 and α-CTF/C83 blots

The detection of β-CTF/C99 and/or α-CTF/C83 in HeLa-APP_{695wt} cells and primary mouse cortical neurons were previously described (Tan and Gleeson, 2019c). Briefly, cell extracts were prepared in 2x reducing sample buffer containing 10% β-mercaptoethanol and boiled at 100^0C. Samples were resolved on 12% NuPAGE^{TM} Bis-Tris SDS-PAGE polyacrylamide gel (Invitrogen, Thermo Fisher Scientific) at 125 V for ~2.5 h. Transfer of proteins onto 0.2 μm nitrocellulose membrane (BIO-RAD) was conducted at 400 mA for 1 h on ice. The membrane was incubated and blocked with 10% w/v skim milk/PBSTween-20 for 1 h at RT to reduce non-specific binding. The membrane was incubated overnight at 4^0C with either W0-2 (detection of β-CTF/C99) or Y188 (detection of β-CTF/C99 and α-CTF/C83) antibodies diluted 1/6000 in PBS Tween-20. The membrane was then incubated with 1/500 diluted secondary antibodies conjugated with horseradish peroxidase (HRP) for 1 h and washed as above.

Quantitative analyses

Quantitation of the colocalization between either BACE1-GFP or Str-Ii_BACE1FL-SBP-EGFP with endogenous organelle markers in HeLa cells was conducted using an organelle-based colocalization (OBCOL) plugin (Woodcroft *et al.*, 2009) in FIJI/ImageJ (NIH public domain software). Quantitation of the average Golgi intensity was carried out using FIJI/ImageJ. Time-lapse videos of cells with z-stacks was projected with maximum intensity projection, and the frames were aligned with "Linear Stack Alignment with SIFT" plugin. A region of interest (ROI) was drawn around the Golgi apparatus, and the average fluorescence intensity over time was measured and recorded for individual cells. The rate of Golgi intensity drop was calculated using linear regression from the maximum Golgi intensity point. The percentage of colocalization of cargo with various organelles was calculated by dividing the total cargo pixels that overlapped with each organelle marker with total cargo pixels within each cell. All analysis was carried out on the indicated number of cells over three independent experiments.

Due to the superiority in image analysis of z-stack images, Imaris microscopy image analysis software (Oxford Instruments) was used over OBCOL to determine the colocalization of endogenous BACE1 with organelle markers in primary cortical neurons at steady-state. Prior to Imaris analyses, confocal images of primary cortical neurons in z-stacks were deconvoluted with the Huygens software (Scientific Volume Imaging) using the default conservative deconvolution setting. Imaris thresholding parameters used were grain size/surface detail of 0.0847 μm, diameter of largest sphere at 0.2 μm and the number of voxels above 10. Imaris surface-surface colocalization tool was used to obtain volume sums of BACE1, organelle marker, and colocalization between BACE1 and the organelle marker. To obtain the percentage of colocalization, the volume sum of colocalization between BACE1 and a specific organelle marker divided by the total volume sum of BACE1. To determine the levels of colocalization of either endogenous BACE1 or APP with endogenous p230/golgin-245 based on pixel intensity in shRNA-treated neurons, Volocity™ imaging software (Perkin Elmer, UK) was used to calculate Manders' coefficient M1 values (Manders, 1993) of either endogenous BACE1 or APP with endogenous p230/golgin-245. All analyses were carried out on the indicated number of cells over three independent experiments.

Generation of graphs and statistical analyses

The generation of graphs and statistical analyses were conducted using Prism (GraphPad Software). Data for fold change of α-CTF/C83 and β-CTF/C99 levels were plotted as bar graphs. Data from

Aβ ELISAs and flow cytometry experiments were plotted as bar graphs and analyzed by unpaired, two-tailed, Student's t-test. Data from quantitation of colocalization, average BACE1 fluorescence intensity and the rate of decrease in BACE1 fluorescence intensity at the Golgi were plotted as dot-plots and analyzed by unpaired, two-tailed, Student's *t*-test. Datasets, involving multiple comparisons to the control, were analyzed by one-way ANOVA using Tukey's multiple comparison test. A *p*-value of <0.05(*) was considered significant, a *p*-value of <0.01(**) was considered highly significant and a *p*-value of <0.001(***) was considered very highly significant.

Acknowledgements: Confocal Microscopy was performed at the Biological Optical Microscopy Platform (BOMP) at the University of Melbourne. This work was supported by funding from the National Health and Medical Research Council of Australia (APP1163862). JZAT and JW are supported by University of Melbourne International Postgraduate Awards. We gratefully acknowledge Fiona Houghton for reagents and expert technical advice, Dr Wei Hong Toh and other members of the Gleeson laboratory for valuable discussions, Allison Van De Meene for maintenance of the spinning disk, Ellie Cho for help for the quantitation and Shirley Taylor for the generation of fluorescent conjugates.

Author Contributions

JZA Tan, L. Fourriere and P. Gleeson conceived the project, designed the experiments, interpreted the data and wrote the manuscript. JZA Tan, L. Fourriere and J Wang performed the experiments and analysed the data. F. Perez and G. Boncompain generated the BACE1 RUSH construct and provided invaluable advice use of the RUSH system.

The authors declare no competing financial interests.

References

Bennett, B.D., Babu-Khan, S., Loeloff, R., Louis, J.C., Curran, E., Citron, M., and Vassar, R. (2000). Expression analysis of BACE2 in brain and peripheral tissues. J Biol Chem *275*, 20647-20651.

Boncompain, G., Divoux, S., Gareil, N., de Forges, H., Lescure, A., Latreche, L., Mercanti, V., Jollivet, F., Raposo, G., and Perez, F. (2012). Synchronization of secretory protein traffic in populations of cells. Nat Methods *9*, 493-498.

Boncompain, G., and Perez, F. (2012). Synchronizing protein transport in the secretory pathway. Curr Protoc Cell Biol *Chapter 15*, Unit 15 19.

Burgos, P.V., Mardones, G.A., Rojas, A.L., daSilva, L.L., Prabhu, Y., Hurley, J.H., and Bonifacino, J.S. (2010). Sorting of the Alzheimer's disease amyloid precursor protein mediated by the AP-4 complex. Dev Cell *18*, 425-436.

Camus, G., Segura-Morales, C., Molle, D., Lopez-Verges, S., Begon-Pescia, C., Cazevieille, C., Schu, P., Bertrand, E., Berlioz-Torrent, C., and Basyuk, E. (2007). The clathrin adaptor complex AP-1 binds HIV-1 and MLV Gag and facilitates their budding. Mol Biol Cell *18*, 3193-3203.

Chen, H.J., Yuan, J., and Lobel, P. (1997). Systematic mutational analysis of the cation-independent mannose 6-phosphate/insulin-like growth factor II receptor cytoplasmic domain. An acidic cluster containing a key aspartate is important for function in lysosomal enzyme sorting. J Biol Chem *272*, 7003-7012.

Chen, Y., Gershlick, D.C., Park, S.Y., and Bonifacino, J.S. (2017). Segregation in the Golgi complex precedes export of endolysosomal proteins in distinct transport carriers. J Cell Biol *216*, 4141-4151.

Chia, P.Z., Toh, W.H., Sharples, R., Gasnereau, I., Hill, A.F., and Gleeson, P.A. (2013). Intracellular itinerary of internalised beta-secretase, BACE1, and its potential impact on beta-amyloid peptide biogenesis. Traffic *14*, 997-1013.

De Matteis, M.A., and Luini, A. (2008). Exiting the Golgi complex. Nat Rev Mol Cell Biol *9*, 273-284.

Donaldson, J.G., and Jackson, C.L. (2011). ARF family G proteins and their regulators: roles in membrane transport, development and disease. Nat Rev Mol Cell Biol *12*, 362-375.

Doray, B., Ghosh, P., Griffith, J., Geuze, H.J., and Kornfeld, S. (2002). Cooperation of GGAs and AP-1 in packaging MPRs at the trans-Golgi network. Science *297*, 1700-1703.

Eng, F.J., Varlamov, O., and Fricker, L.D. (1999). Sequences within the cytoplasmic domain of gp180/carboxypeptidase D mediate localization to the trans-Golgi network. Mol Biol Cell *10*, 35-46.

Farias, G.G., Cuitino, L., Guo, X., Ren, X., Jarnik, M., Mattera, R., and Bonifacino, J.S. (2012). Signal-mediated, AP-1/clathrin-dependent sorting of transmembrane receptors to the somatodendritic domain of hippocampal neurons. Neuron *75*, 810-823.

Feng, T., Tammineni, P., Agrawal, C., Jeong, Y.Y., and Cai, Q. (2017). Autophagy-mediated Regulation of BACE1 Protein Trafficking and Degradation. J Biol Chem *292*, 1679-1690.

Gravotta, D., Carvajal-Gonzalez, J.M., Mattera, R., Deborde, S., Banfelder, J.R., Bonifacino, J.S., and Rodriguez-Boulan, E. (2012). The clathrin adaptor AP-1A mediates basolateral polarity. Dev Cell *22*, 811-823.

He, X., Chang, W.P., Koelsch, G., and Tang, J. (2002). Memapsin 2 (beta-secretase) cytosolic domain binds to the VHS domains of GGA1 and GGA2: implications on the endocytosis mechanism of memapsin 2. FEBS Lett *524*, 183-187.

He, X., Li, F., Chang, W.P., and Tang, J. (2005). GGA proteins mediate the recycling pathway of memapsin 2 (BACE). J Biol Chem *280*, 11696-11703.

Hille-Rehfeld, A. (1995). Mannose 6-phosphate receptors in sorting and transport of lysosomal enzymes. Biochim Biophys Acta *1241*, 177-194.

Hirst, J., Borner, G.H., Antrobus, R., Peden, A.A., Hodson, N.A., Sahlender, D.A., and Robinson, M.S. (2012). Distinct and overlapping roles for AP-1 and GGAs revealed by the "knocksideways" system. Curr Biol *22*, 1711-1716.

Houghton, F.J., Bellingham, S.A., Hill, A.F., Bourges, D., Ang, D.K., Gemetzis, T., Gasnereau, I., and Gleeson, P.A. (2012). Arl5b is a Golgi-localised small G protein involved in the regulation of retrograde transport. Exp Cell Res *318*, 464-477.

Huse, J.T., Liu, K., Pijak, D.S., Carlin, D., Lee, V.M., and Doms, R.W. (2002). Beta-secretase processing in the trans-Golgi network preferentially generates truncated amyloid species that accumulate in Alzheimer's disease brain. J Biol Chem *277*, 16278-16284.

Huse, J.T., Pijak, D.S., Leslie, G.J., Lee, V.M., and Doms, R.W. (2000). Maturation and endosomal targeting of beta-site amyloid precursor protein-cleaving enzyme. The Alzheimer's disease beta-secretase. J Biol Chem *275*, 33729-33737.

Hussain, I., Powell, D., Howlett, D.R., Tew, D.G., Meek, T.D., Chapman, C., Gloger, I.S., Murphy, K.E., Southan, C.D., Ryan, D.M., Smith, T.S., Simmons, D.L., Walsh, F.S., Dingwall, C., and Christie, G. (1999). Identification of a novel aspartic protease (Asp 2) as beta-secretase. Mol Cell Neurosci *14*, 419-427.

Kinoshita, A., Fukumoto, H., Shah, T., Whelan, C.M., Irizarry, M.C., and Hyman, B.T. (2003). Demonstration by FRET of BACE interaction with the amyloid precursor protein at the cell surface and in early endosomes. J Cell Sci *116*, 3339-3346.

Kooy, J., Toh, B.H., Pettitt, J.M., Erlich, R., and Gleeson, P.A. (1992). Human autoantibodies as reagents to conserved Golgi components. Characterization of a peripheral, 230-kDa compartment-specific Golgi protein. J Biol Chem *267*, 20255-20263.

Lane, C.A., Hardy, J., and Schott, J.M. (2017). Alzheimer's disease. Eur J Neurol *0*, 1-12.

Le Borgne, R., and Hoflack, B. (1997). Mannose 6-phosphate receptors regulate the formation of clathrin-coated vesicles in the TGN. J Cell Biol *137*, 335-345.

Lee, I., Doray, B., Govero, J., and Kornfeld, S. (2008). Binding of cargo sorting signals to AP-1 enhances its association with ADP ribosylation factor 1-GTP. J Cell Biol *180*, 467-472.

Lowery, J., Szul, T., Styers, M., Holloway, Z., Oorschot, V., Klumperman, J., and Sztul, E. (2013). The Sec7 guanine nucleotide exchange factor GBF1 regulates membrane recruitment of BIG1 and BIG2 guanine nucleotide exchange factors to the trans-Golgi network (TGN). J Biol Chem *288*, 11532-11545.

Luke, M.R., Kjer-Nielsen, L., Brown, D.L., Stow, J.L., and Gleeson, P.A. (2003). GRIP domain-mediated targeting of two new coiled-coil proteins, GCC88 and GCC185, to subcompartments of the trans-Golgi network. Journal of Biological Chemistry *278*, 4216-4226.

Manders, E.M.M., Verbeek, F. J. and Aten, J. A. (1993). Measurement of co-localization of objects in dual-colour confocal images. Journal of Microscopy *169*, 375–382.

Meyer, C., Zizioli, D., Lausmann, S., Eskelinen, E.L., Hamann, J., Saftig, P., von Figura, K., and Schu, P. (2000). mu1A-adaptin-deficient mice: lethality, loss of AP-1 binding and rerouting of mannose 6-phosphate receptors. EMBO J *19*, 2193-2203.

Nakai, W., Kondo, Y., Saitoh, A., Naito, T., Nakayama, K., and Shin, H.W. (2013). ARF1 and ARF4 regulate recycling endosomal morphology and retrograde transport from endosomes to the Golgi apparatus. Mol Biol Cell *24*, 2570-2581.

Navarro Negredo, P., Edgar, J.R., Wrobel, A.G., Zaccai, N.R., Antrobus, R., Owen, D.J., and Robinson, M.S. (2017). Contribution of the clathrin adaptor AP-1 subunit micro1 to acidic cluster protein sorting. J Cell Biol *216*, 2927-2943.

Prabhu, Y., Burgos, P.V., Schindler, C., Farias, G.G., Magadan, J.G., and Bonifacino, J.S. (2012). Adaptor protein 2-mediated endocytosis of the beta-secretase BACE1 is dispensable for amyloid precursor protein processing. Mol Biol Cell *23*, 2339-2351.

Qi-Takahara, Y., Morishima-Kawashima, M., Tanimura, Y., Dolios, G., Hirotani, N., Horikoshi, Y., Kametani, F., Maeda, M., Saido, T.C., Wang, R., and Ihara, Y. (2005). Longer forms of amyloid beta protein: implications for the mechanism of intramembrane cleavage by gamma-secretase. J Neurosci *25*, 436-445.

Rechards, M., Xia, W., Oorschot, V.M., Selkoe, D.J., and Klumperman, J. (2003). Presenilin-1 exists in both pre- and post-Golgi compartments and recycles via COPI-coated membranes. Traffic *4*, 553-565.

Reiling, J.H., Olive, A.J., Sanyal, S., Carette, J.E., Brummelkamp, T.R., Ploegh, H.L., Starnbach, M.N., and Sabatini, D.M. (2013). A CREB3-ARF4 signalling pathway mediates the response to Golgi stress and susceptibility to pathogens. Nat Cell Biol *15*, 1473-1485.

Scherer, W.F., Syverton, J.T., and Gey, G.O. (1953). Studies on the propagation in vitro of poliomyelitis viruses. IV. Viral multiplication in a stable strain of human malignant epithelial cells (strain HeLa) derived from an epidermoid carcinoma of the cervix. J Exp Med *97*, 695-710.

Schieb, H., Kratzin, H., Jahn, O., Mobius, W., Rabe, S., Staufenbiel, M., Wiltfang, J., and Klafki, H.W. (2011). Beta-amyloid peptide variants in brains and cerebrospinal fluid from amyloid precursor protein (APP) transgenic mice: comparison with human Alzheimer amyloid. J Biol Chem *286*, 33747-33758.

Schneider, C., Sutherland, R., Newman, R., and Greaves, M. (1982). Structural features of the cell surface receptor for transferrin that is recognized by the monoclonal antibody OKT9. J Biol Chem *257*, 8516-8522.

Shimizu, H., Tosaki, A., Kaneko, K., Hisano, T., Sakurai, T., and Nukina, N. (2008). Crystal structure of an active form of BACE1, an enzyme responsible for amyloid beta protein production. Mol Cell Biol *28*, 3663-3671.

Sinha, S., Anderson, J.P., Barbour, R., Basi, G.S., Caccavello, R., Davis, D., Doan, M., Dovey, H.F., Frigon, N., Hong, J., Jacobson-Croak, K., Jewett, N., Keim, P., Knops, J., Lieberburg, I., Power, M., Tan, H., Tatsuno, G., Tung, J., Schenk, D., Seubert, P., Suomensaari, S.M., Wang, S., Walker, D., Zhao, J., McConlogue, L., and John, V. (1999). Purification and cloning of amyloid precursor protein beta-secretase from human brain. Nature *402*, 537-540.

Southon, A., Greenough, M., Hung, Y.H., Norgate, M., Burke, R., and Camakaris, J. (2011). The ADP-ribosylation factor 1 (Arf1) is involved in regulating copper uptake. Int J Biochem Cell Biol *43*, 146-153.

Stamnes, M.A., and Rothman, J.E. (1993). The binding of AP-1 clathrin adaptor particles to Golgi membranes requires ADP-ribosylation factor, a small GTP-binding protein. Cell *73*, 999-1005.

Takami, M., Nagashima, Y., Sano, Y., Ishihara, S., Morishima-Kawashima, M., Funamoto, S., and Ihara, Y. (2009). gamma-Secretase: successive tripeptide and tetrapeptide release from the transmembrane domain of beta-carboxyl terminal fragment. J Neurosci *29*, 13042-13052.

Tan, J.Z.A., and Gleeson, P.A. (2019a). Cargo Sorting at the trans-Golgi Network for Shunting into Specific Transport Routes: Role of Arf Small G Proteins and Adaptor Complexes. Cells *8*.

Tan, J.Z.A., and Gleeson, P.A. (2019b). The role of membrane trafficking in the processing of amyloid precursor protein and production of amyloid peptides in Alzheimer's disease. Biochim Biophys Acta Biomembr *1861*, 697-712.

Tan, J.Z.A., and Gleeson, P.A. (2019c). The trans-Golgi network is a major site for alpha-secretase processing of amyloid precursor protein in primary neurons. J Biol Chem *294*, 1618-1631.

Thinakaran, G., and Koo, E.H. (2008). Amyloid precursor protein trafficking, processing, and function. J Biol Chem *283*, 29615-29619.

Toh, W.H., Chia, P.Z.C., Hossain, M.I., and Gleeson, P.A. (2018). GGA1 regulates signal-dependent sorting of BACE1 to recycling endosomes which moderates Abeta production. Mol Biol Cell *29*, 191-208.

Toh, W.H., and Gleeson, P.A. (2016). Dysregulation of intracellular trafficking and endosomal sorting in Alzheimer's disease: controversies and unanswered questions. Biochem J *473*, 1977-1993.

Toh, W.H., Tan, J.Z., Zulkefli, K.L., Houghton, F.J., and Gleeson, P.A. (2017). Amyloid precursor protein traffics from the Golgi directly to early endosomes in an Arl5b- and AP4-dependent pathway. Traffic *18*, 159-175.

Tomita, T. (2014). Molecular mechanism of intramembrane proteolysis by gamma-secretase. J Biochem *156*, 195-201.

Voorhees, P., Deignan, E., van Donselaar, E., Humphrey, J., Marks, M.S., Peters, P.J., and Bonifacino, J.S. (1995). An acidic sequence within the cytoplasmic domain of furin functions as a determinant of trans-Golgi network localization and internalization from the cell surface. EMBO J *14*, 4961-4975.

Woodcroft, B.J., Hammond, L., Stow, J.L., and Hamilton, N.A. (2009). Automated organelle-based colocalization in whole-cell imaging. Cytometry A *75*, 941-950.

Yan, R., Bienkowski, M.J., Shuck, M.E., Miao, H., Tory, M.C., Pauley, A.M., Brashier, J.R., Stratman, N.C., Mathews, W.R., Buhl, A.E., Carter, D.B., Tomasselli, A.G., Parodi, L.A., Heinrikson, R.L., and Gurney, M.E. (1999). Membrane-anchored aspartyl protease with Alzheimer's disease beta-secretase activity. Nature *402*, 533-537.

Ye, X., and Cai, Q. (2014). Snapin-mediated BACE1 retrograde transport is essential for its degradation in lysosomes and regulation of APP processing in neurons. Cell Rep *6*, 24-31.

Ye, X., Feng, T., Tammineni, P., Chang, Q., Jeong, Y.Y., Margolis, D.J., Cai, H., Kusnecov, A., and Cai, Q. (2017). Regulation of Synaptic Amyloid-beta Generation through BACE1 Retrograde Transport in a Mouse Model of Alzheimer's Disease. J Neurosci *37*, 2639-2655.

Zhang, Y.W., Thompson, R., Zhang, H., and Xu, H. (2011). APP processing in Alzheimer's disease. Mol Brain *4*, 3.

Legends to figures

Figure 1 Anterograde trafficking of BACE1

(**A**) A schematic outlining the experimental plan to investigate the post-Golgi trafficking of BACE1 using the RUSH system. BACE1-SBP-GFP is retained in the ER compartment via interaction of its SBP with streptavidin fused ER hook protein. BACE1-SBP-GFP is released from the ER upon biotin addition to allow trafficking of BACE1-SBP-GFP to its target compartment.

(**B**) HeLa cells were transiently transfected with the BACE1-SBP-GFP and ER hook bicistronic construct for 24 h. Transfected HeLa cells were treated with biotin (untreated represents the 0 min time point) and incubated at 37^0C. Monolayers of HeLa cells were fixed at the indicated time points, then permeabilized and blocked, followed by staining with either mouse anti-EEA1 (red) and rabbit anti-GCC88 (far-red converted to red), mouse anti-Rab11 (red), or mouse anti-CD63 (red) antibodies, and DAPI (blue). Inset represents magnified images. Bar represents 10 μm.

(**C**) The percentage of BACE1-GFP at the TGN, early endosomes, recycling endosomes and late endosomes were calculated as a percentage of total BACE1-GFP pixels that overlapped with GCC88, EEA1, Rab11, and CD63, respectively, using the OBCOL plugin on ImageJ. The steady state distribution of BACE1-SBP-GFP was determined from transfected HeLa cells incubated for 24 h in the continuous presence of biotin. Data are represented as the mean ± SD of 3 independent experiments (n=15).

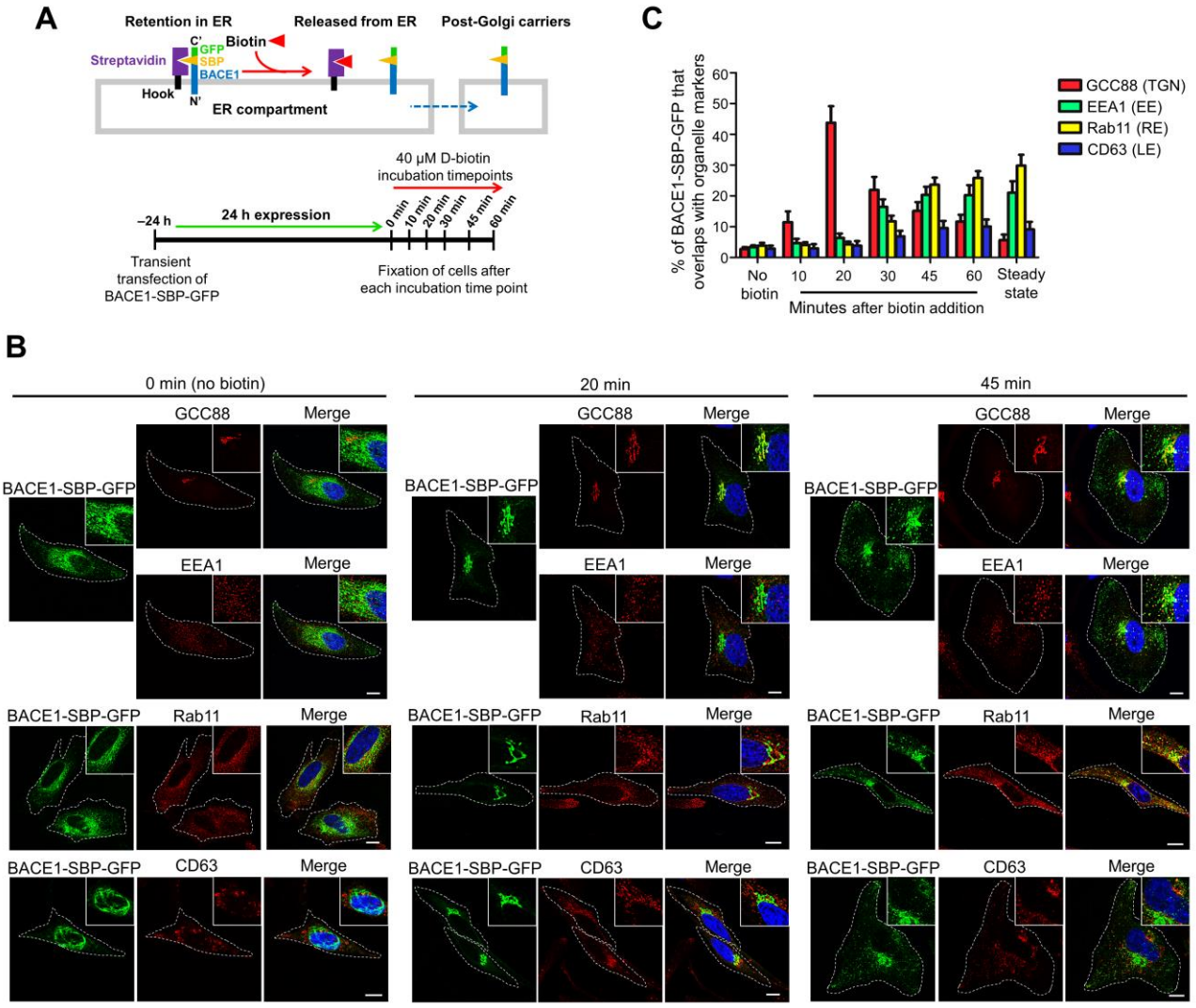
A
Retention in ER
Released from ER
Post-Golgi carriers
C'
GFP
SBP
BACE1
Biotin
Streptavidin
Hook
N'
ER compartment
40 µM D-biotin
incubation timepoints
–24 h
24 h expression
0 min
10 min
20 min
30 min
45 min
60 min
Transient
transfection of
BACE1-SBP-GFP
Fixation of cells after
each incubation time point
C
% of BACE1-SBP-GFP that
overlaps with organelle markers
GCC88 (TGN)
EEA1 (EE)
Rab11 (RE)
CD63 (LE)
No
biotin
10
20
30
45
60
Steady
state
Minutes after biotin addition
B
0 min (no biotin)
20 min
45 min
GCC88
Merge
BACE1-SBP-GFP
EEA1
Rab11
CD63

Figure 2 Post-Golgi trafficking of newly synthesized BACE1

HeLa cells were transiently transfected with the BACE1-SBP-GFP and ER hook bicistronic construct for 24 h. (**A)** Real time images were acquired using a TIRF microscope at the indicated time points. Biotin was added at time 0 min. Scale bar represents 5µm. (**B**) Fast image acquisition of BACE1-SBP-GFP. Images were acquired every 2 sec. Temporal projection was performed from 15 min to 45 min using the tool "temporal-color-code" on the Fiji software. Bar represents 5 µm.

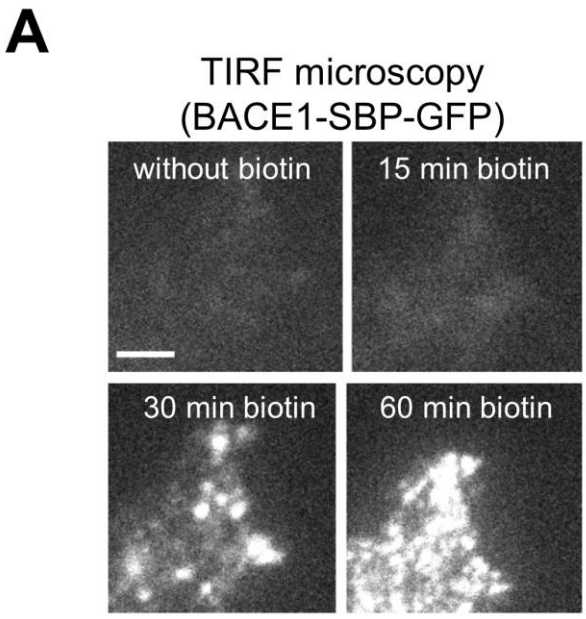

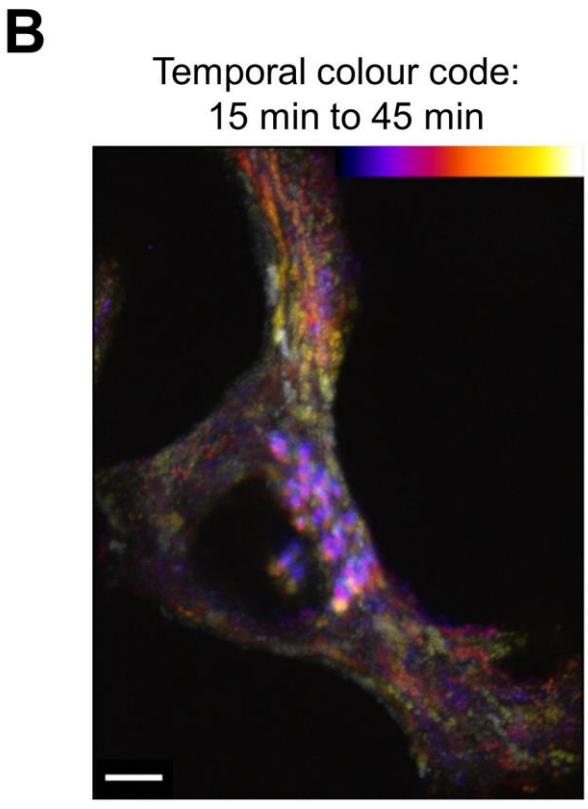

Figure 3 Steady-state distribution of BACE1 in HeLa cells and primary neurons

(**A**) HeLa cells stably expressing BACE1-GFP were fixed, permeabilized and blocked, followed by staining with either rabbit anti-GCC88 (far-red converted to red/green) and mouse anti-Rab11 (red), mouse anti-EEA1 (red), or mouse anti-CD63 (red) antibodies, and DAPI (blue). Insets and higher magnification of the images of the cells marked * are also shown. Bars represents 10 μm.

(**B**) The percentage of BACE1-GFP at the TGN, recycling endosomes, early endosomes, and late endosomes/lysosomes were calculated as a percentage of total BACE1-GFP pixels that overlapped with GCC88, Rab11, EEA1, and CD63, respectively, using the OBCOL plugin on ImageJ. Data are represented as the mean±SD of 3 independent experiments (n=16).

(**C**) Primary mouse cortical neurons at DIV7 were stained with anti-rabbit BACE1 for endogenous BACE1 (green) and either human anti-p230/golgin-245 (red), rat anti-LAMP1 (red), mouse anti-Rab11 (red) or anti-Rab4 (red) antibodies overnight at 4^0C. Higher magnification of the merged images are also shown. Bar represents 10 μm.

(**D**) The percentage of endogenous BACE1 at the TGN, recycling endosomes, early endosomes, and late endosomes/lysosomes in neurons were calculated as a percentage of volume sum of BACE1 that overlapped with p230/golgin-245, Rab11, Rab4, and LAMP1, respectively, using Imaris. Data are represented as the mean ± SD of 3 independent experiments (n=13-14).

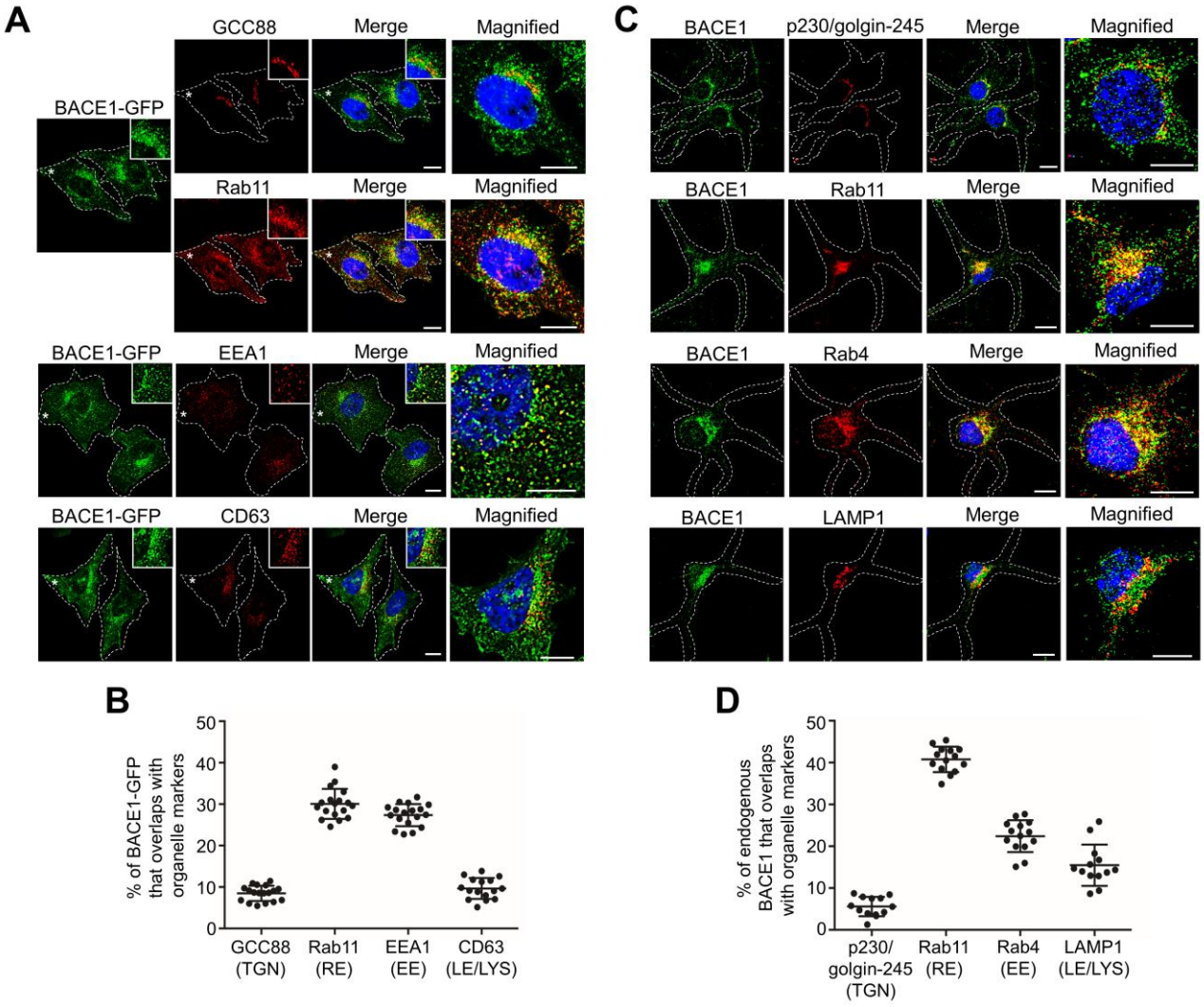
A
BACE1-GFP
GCC88
Merge
Magnified
Rab11
EEA1
CD63
C
BACE1
p230/golgin-245
Rab4
LAMP1
B
% of BACE1-GFP that overlaps with organelle markers
0
10
20
30
40
50
GCC88 (TGN)
Rab11 (RE)
EEA1 (EE)
CD63 (LE/LYS)
D
% of endogenous BACE1 that overlaps with organelle markers
p230/ golgin-245 (TGN)
Rab4 (EE)
LAMP1 (LE/LYS)

Figure 4 Depletion of adaptor protein AP-1 results in BACE1 accumulation in the TGN

(**A**) HeLa cells stably expressing BACE1-GFP were transfected with either control siRNA, AP-1γ siRNA, GGA1 siRNA, AP-4ε siRNA or Arl5b siRNA for 72 h. (**B**) HeLa cells stably expressing Arl5b(Q70L)-GFP were transfected with either control siRNA or Arl5b siRNA for 72 h. (**A and B**) Cells were lysed in RIPA buffer, and 20 μg of cell extracts were subjected to SDS-PAGE on 4–12% gradient polyacrylamide gel. Proteins were transferred to a PVDF membrane and probed with (**A**) mouse anti-AP-1γ, rabbit anti-GGA1, mouse anti-AP-4ε, (**B**) mouse anti-GFP and (**A and B**) mouse anti-α-tubulin antibodies using a chemiluminescence detection system. (**C**) Monolayers of HeLa cells were fixed, permeabilized and blocked, followed by staining with mouse anti-Golgin-97 antibodies (red) and DAPI (blue). Higher magnification of the merged images of the cells marked * are also shown. Bar represents 10 μm. (**D**) The percentage of BACE1-GFP at the TGN was calculated as a percentage of total BACE1-GFP pixels that overlapped with Golgin-97. Data are represented as the mean ± SD of 3 independent experiments (n=15) and analyzed by one-way ANOVA using Tukey's test. *** $p < 0.001$.

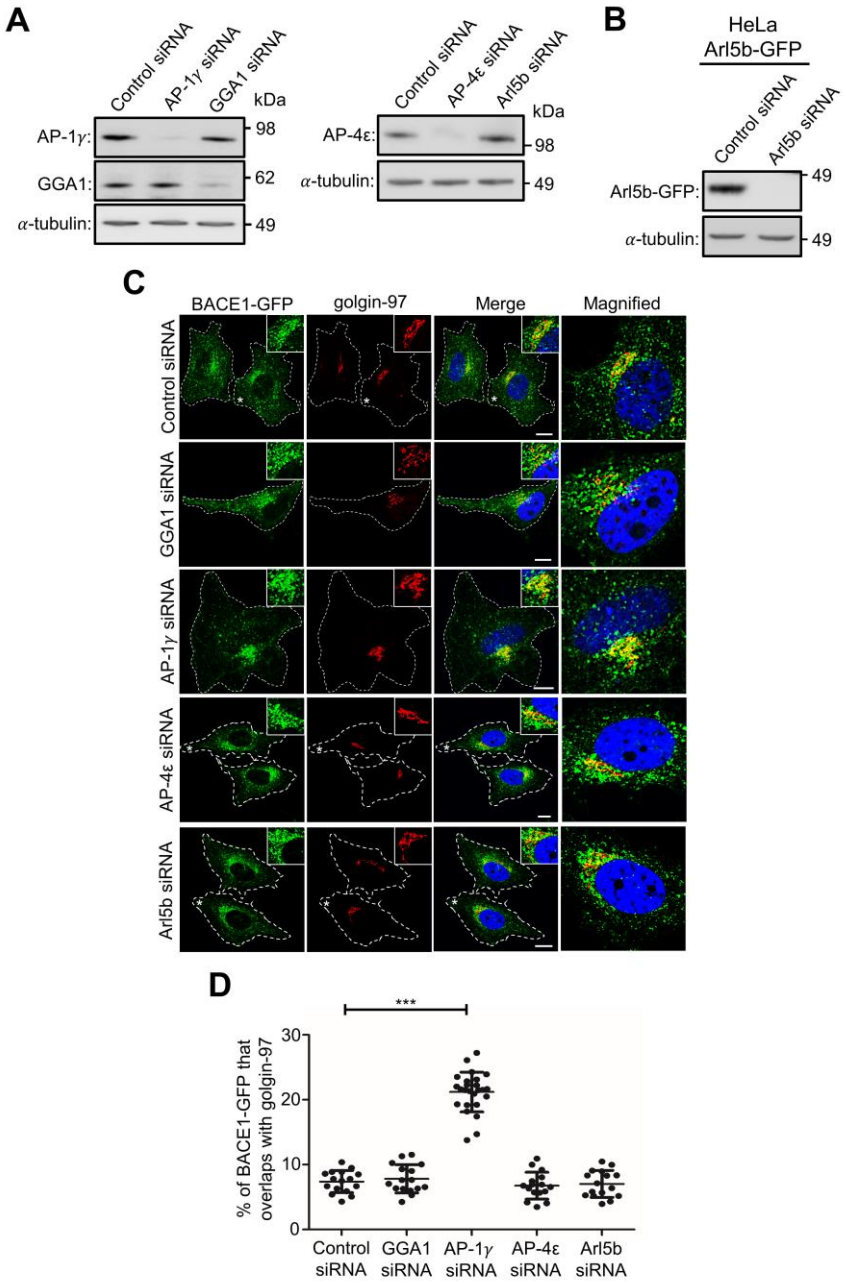
A
Control siRNA
AP-1γ siRNA
GGA1 siRNA
kDa
AP-1γ:
GGA1:
α-tubulin:
98
62
49
Control siRNA
AP-4ε siRNA
Arl5b siRNA
kDa
AP-4ε:
α-tubulin:
98
49
B
HeLa
Arl5b-GFP
Control siRNA
Arl5b siRNA
Arl5b-GFP:
α-tubulin:
49
49
C
BACE1-GFP
golgin-97
Merge
Magnified
Control siRNA
GGA1 siRNA
AP-1γ siRNA
AP-4ε siRNA
Arl5b siRNA
D
***
% of BACE1-GFP that overlaps with golgin-97
30
20
10
0
Control siRNA
GGA1 siRNA
AP-1γ siRNA
AP-4ε siRNA
Arl5b siRNA

Figure 5 Depletion of AP-1 results in a reduction of BACE1 in the recycling endosomes

(**A**) HeLa cells stably expressing BACE1-GFP were transfected with either control siRNA or AP-1γ siRNA for 72 h. Cells were fixed and stained with mouse anti-Rab11 antibodies (red) and DAPI (blue). Higher magnification of the merged images are also shown. Bar represents 10 μm. (**B**) Data are represented as the mean ± SD of 3 independent experiments (n=24) and analyzed by unpaired, two-tailed Student's *t*-test. *** $p < 0.001$.

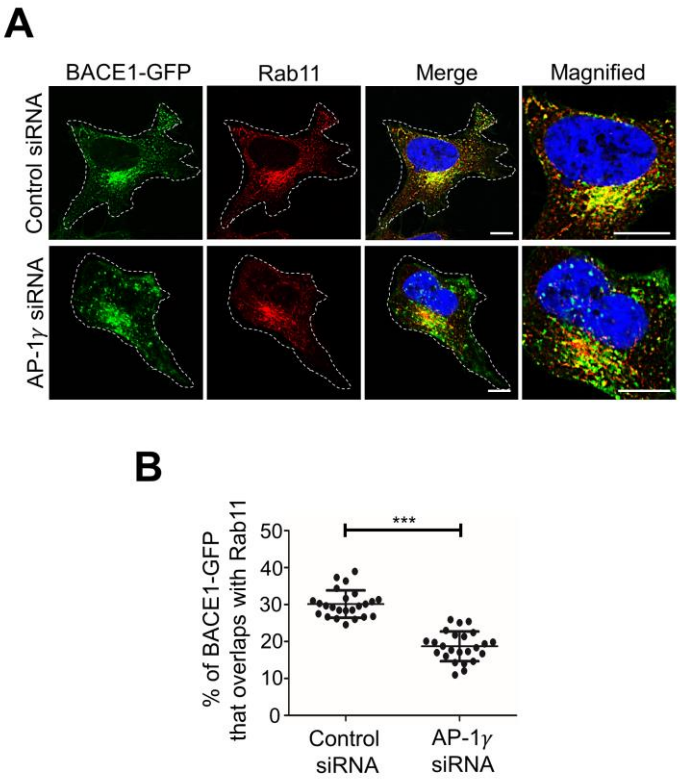

Figure 6 Depletion of* AP-1γ *in mouse primary cortical neurons results in accumulation of BACE1 in the TGN

(**A** and **C**) Transduction of E16 primary mouse cortical neurons at DIV3 with either AP-1γ shRNA or AP-4ε shRNA recombinant lentivirus for 96 h. Neurons were fixed at DIV7 and stained with either (**A**) rabbit anti-BACE1 (far-red converted to green) or (**C**) rabbit anti-APP (Y188; red), and the TGN marker, human anti-p230/golgin-245 (red/ far-red converted to green) antibodies overnight at 4^0C. Nuclei was stained with DAPI (blue). Bar represents 10 µm. (**B** and **D**) Volocity™ software was used to calculate Manders' coefficient M1 values of either BACE1 or APP colocalization with the TGN marker, p230/golgin-245. Data are represented as the mean ± SD of 3 independent experiments (n=14–15 individual cells) and analyzed by (**B**) one-way ANOVA using Tukey's test and (**D**) unpaired, two-tailed Student's *t*-test. ***p<0.001 and n.s.=not significant.

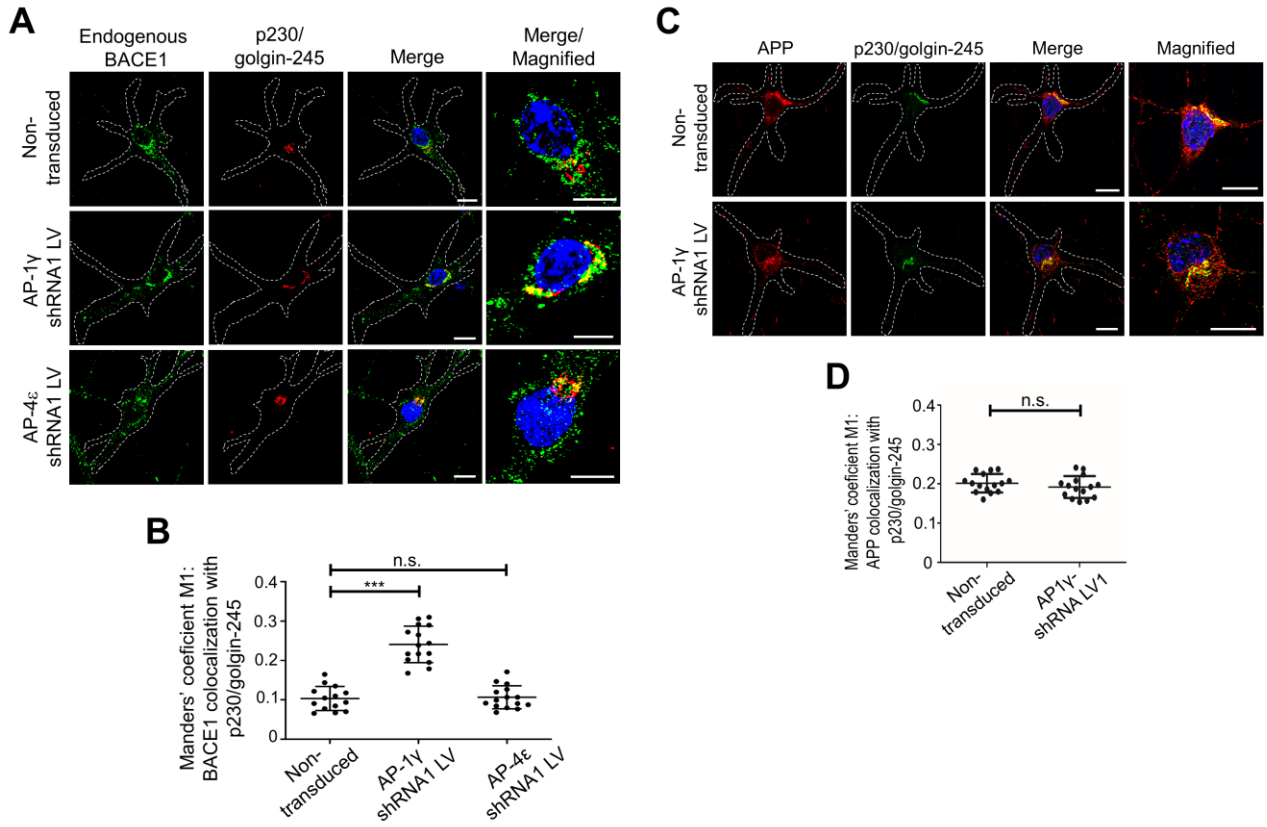

Figure 7 Delayed exit of RUSH-BACE1-GFP from the TGN by AP-1 depletion

(**A** and **B**) HeLa cells were transfected with either control siRNA, AP-1γ siRNA or AP-4ε siRNA for 72 h. Cells were co-transfected with Str-Ii_BACE1-SBP-GFP after 48 h for a further 24 h before live imaging at 37°C. Biotin was added at 0 min, and (**A**) images at the indicated time-points after biotin addition are shown. Bar represents 10 μm. (**B**) Representative curves of mean Golgi-region intensity change over time. Images were taken every 1 min for a duration of 60 min. Mean intensity over Golgi-region of individual cells was measured over time after biotin addition using FIJI/ImageJ. The level of (**C**) maximal Golgi-region intensity and the (**D**) corresponding time-point were recorded and quantified from the curves in (**B**). (**E**) The rate of Golgi-region intensity drop was quantified from (**B**). Linear regression of the curve starting from the maximal intensity point over the next 20 min was generated, and the slope was recorded as a measure of BACE1 Golgi exit rate. (**C**-**E**) Data are presented as mean ± SD of 3 independent experiments (n = 18–23) and analyzed by one-way ANOVA using Tukey's test. ** $p < 0.01$ and n.s.=not significant.

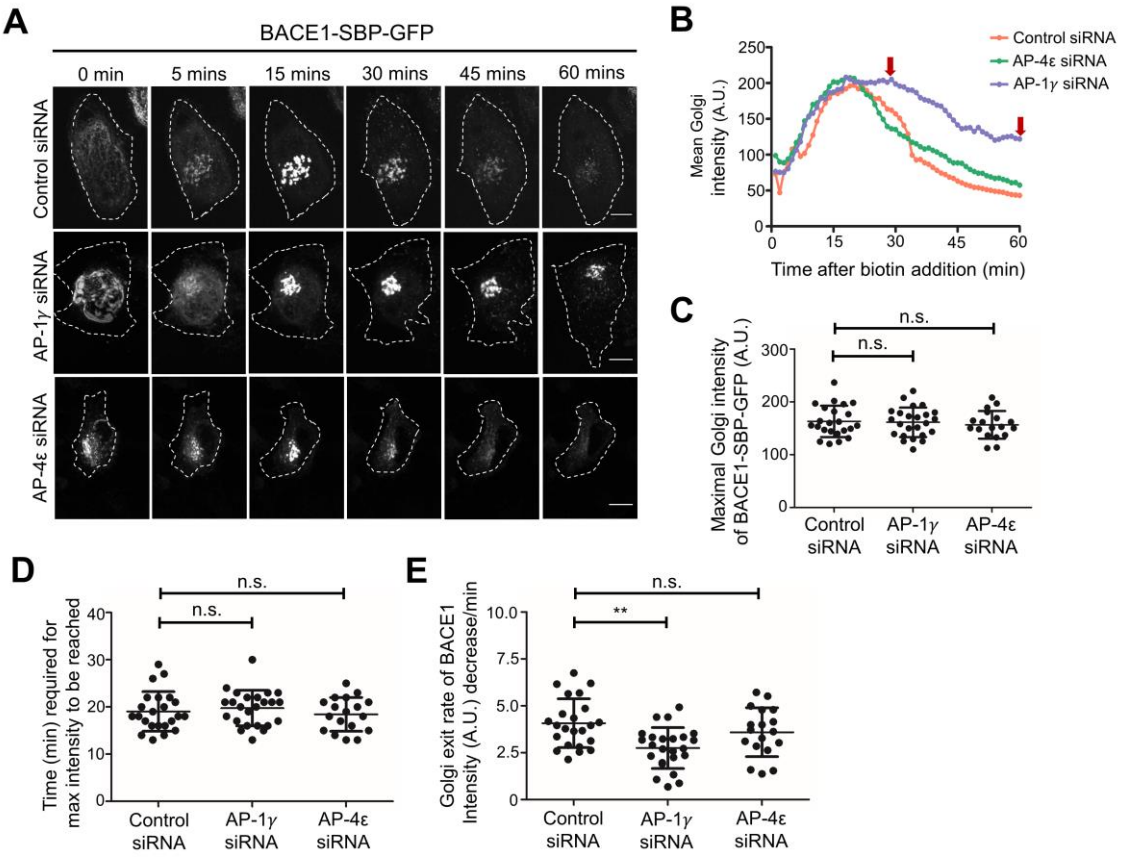

Figure 8 Depletion of small G protein Arf1 and Arf4 results in BACE1 accumulation in the TGN

HeLa cells stably expressing BACE1-GFP were transfected with either control siRNA, AP-1γ siRNA, Arf1 siRNA, Arf4 siRNA, or Arf1+4 siRNAs for 72 h. (**A**) Cells were lysed in RIPA buffer, and 20 μg of cell extracts were subjected to SDS-PAGE on 4–12% gradient polyacrylamide gel. Proteins were transferred to a PVDF membrane and probed with mouse anti-AP-1γ, mouse anti-α-tubulin, and either mouse anti-Arf1 or rabbit anti-Arf4 antibodies on a duplicated blot using a chemiluminescence detection system. (**B**) Cells transfected with Arf1 siRNA and Arf4 siRNA were also co-transfected with Arf1(WT)-mCherry and Arf4(WT)-mCherry construct, respectively, 48 h later for a further 24 h, as indicated. (**B & C**) Monolayers of HeLa cells were fixed, permeabilized and blocked, followed by staining with mouse anti-golgin-97 antibodies (red/far-red converted to red) and DAPI (blue). Higher magnification of the merged images of the cells marked * are also shown. Inset represents magnified images for Arf1 and Arf4 rescue experiments. Bar represents 10 μm. (**D–F**) The percentage of BACE1-GFP at the TGN was calculated as a percentage of total BACE1-GFP pixels that overlapped with golgin-97. Data are represented as the mean ± SD of 3 independent experiments (n=15–25) and analyzed by (**D**) one-way ANOVA using Tukey's test and (**E & F**) unpaired, two-tailed Student's *t*-test. *** $p < 0.001$ and ** $p < 0.01$.

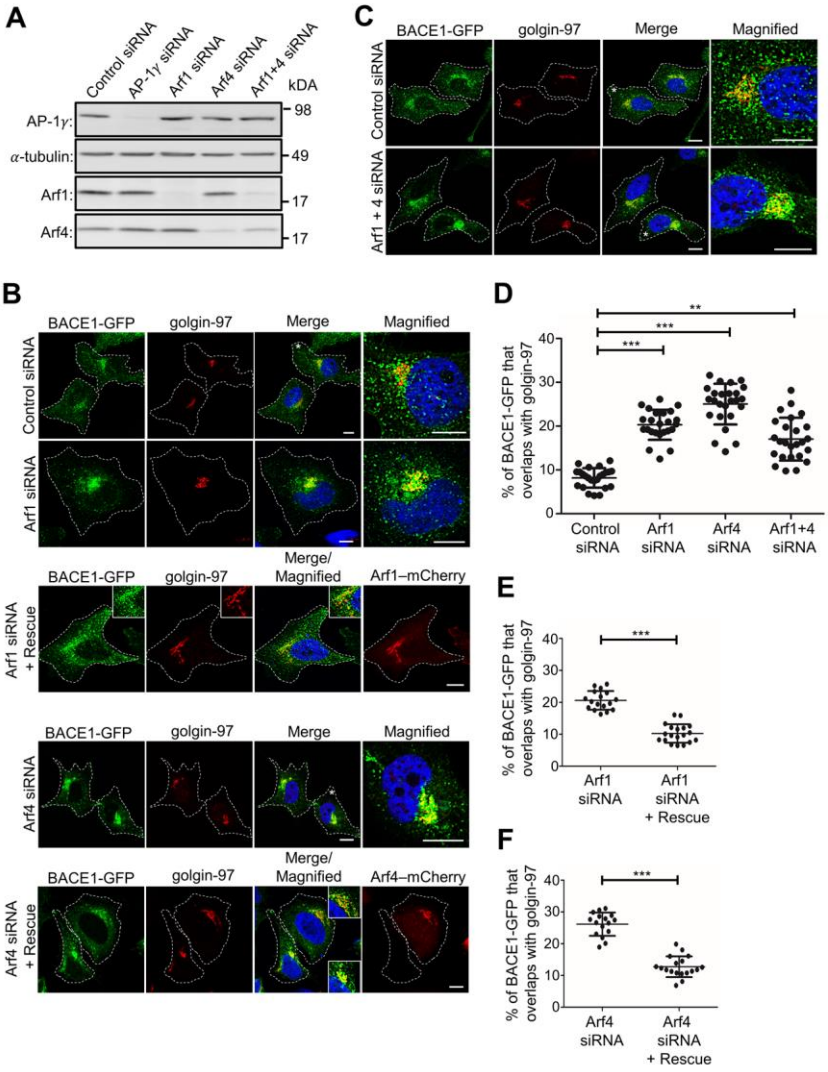
A
Control siRNA
AP-1γ siRNA
Arf1 siRNA
Arf4 siRNA
Arf1+4 siRNA
kDA
AP-1γ:
α-tubulin:
Arf1:
Arf4:
98
49
17
17
B
BACE1-GFP
golgin-97
Merge
Magnified
Control siRNA
Arf1 siRNA
Merge/
Magnified
Arf1–mCherry
Arf1 siRNA
+ Rescue
Arf4 siRNA
Arf4–mCherry
Arf4 siRNA
+ Rescue
C
BACE1-GFP
golgin-97
Merge
Magnified
Control siRNA
Arf1 + 4 siRNA
D
% of BACE1-GFP that
overlaps with golgin-97
**
***
***
Control
siRNA
Arf1
siRNA
Arf4
siRNA
Arf1+4
siRNA
E
% of BACE1-GFP that
overlaps with golgin-97
***
Arf1
siRNA
Arf1
siRNA
+ Rescue
F
% of BACE1-GFP that
overlaps with golgin-97
***
Arf4
siRNA
Arf4
siRNA
+ Rescue

Figure 9 AP-1, Arf1 and Arf4 regulates trafficking of BACE1 to the cell surface

HeLa cells stably expressing BACE1-GFP were transfected with either control siRNA (**A**) or AP-1γ siRNA, (**B**) AP-4ε siRNA or Arl5b siRNA, (**C**) Arf1 siRNA, Arf4 siRNA or Arf1+4 siRNAs for 72 h. (**A–C**) Cells were harvested and stained with anti-BACE1 antibodies on ice for 30 min, then fixed in 4% PFA, quenched in 50 mM NH_4Cl and blocked in 5% FCS/PBS without permeabilization. Cell surface BACE1 was stained with Alexa568-conjugated IgG. 10, 000 events were analyzed per sample by flow cytometry. Data analyses and histograms were constructed using Flowjo. (**D–F**) Bar graph showing arbitrary mean fluorescence intensity of cell surface BACE1 in control and (**D**) AP-1γ, (**E**) AP-4ε and Arl5b, (**F**) Arf1 and Arf4 depleted conditions. Data are represented as the mean ± SEM of 3 independent experiments and analyzed by one-way ANOVA using Tukey's test. *** $p < 0.001$ and n.s.=not significant.

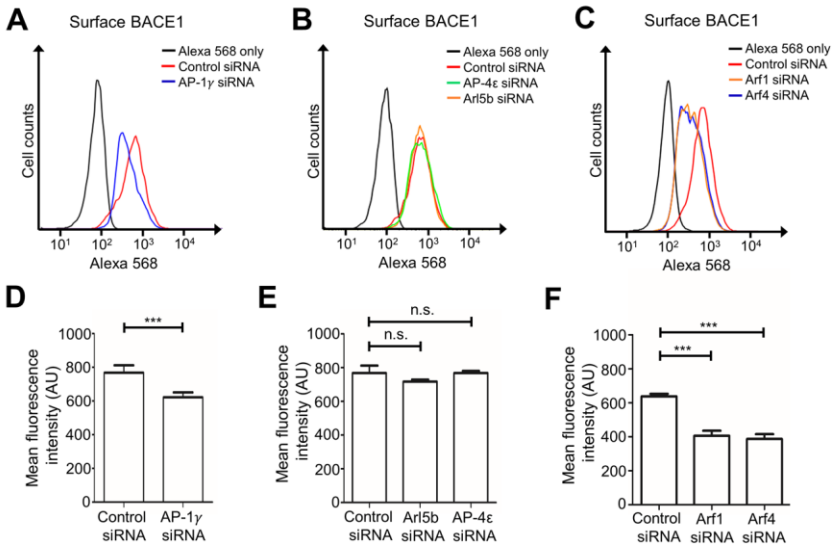

Figure 10 APP processing and Aß production is increased in AP-1, Arf1, Arf4 and Arf1+4 depleted HeLa cells

(**A & B**) HeLa cells stably expressing APP_{695wt} were transfected with either control siRNA (**A**) or AP1γ siRNA, (**B**) Arf1 siRNA, Arf4 siRNA, or Arf1+4 siRNAs; 56 h after transfection the medium was changed and conditioned medium collected 16 h later and analyzed for secreted Aβ using a sandwich ELISA specific for Aβ40. The Aβ40 levels for each sample were normalized against the total cellular protein. Data are represented as the mean ± SEM of 3 independent experiments and analyzed by (**A**) unpaired, two-tailed Student's *t*-test and (**B**) one-way ANOVA using Tukey's test. ***p<0.001 and **p<0.01. (**C, D**) HeLa cells stably expressing APP_{695wt} were transfected with either control siRNA, AP-1γ siRNA (**C**), Arf1 siRNA, Arf4 siRNA, or Arf1+4 siRNAs (**D**) for 72 h and then treated with either DMSO (carrier control) or 250 nM γ-secretase inhibitor DAPT in the last 16 h of siRNA transfection. Cells were lysed, and 20 µg of cell extracts per sample were subjected to SDS-PAGE. Proteins were transferred onto either PVDF and probed with mouse antibodies to AP-4ε or α-tubulin, or nitrocellulose membrane and probed with mouse W02 antibodies to β-CTF/C99. (**E**) Bar graph representing fold change of β-CTF/C99 levels in AP-1γ siRNA, Arf1 siRNA, Arf4 siRNA, and Arf1+4 siRNAs compared to control siRNA. Data are represented as the mean ± SD of 4 independent experiments and analyzed by one-way ANOVA using Tukey's test. ***p<0.001, **p<0.01 and *p<0.05.

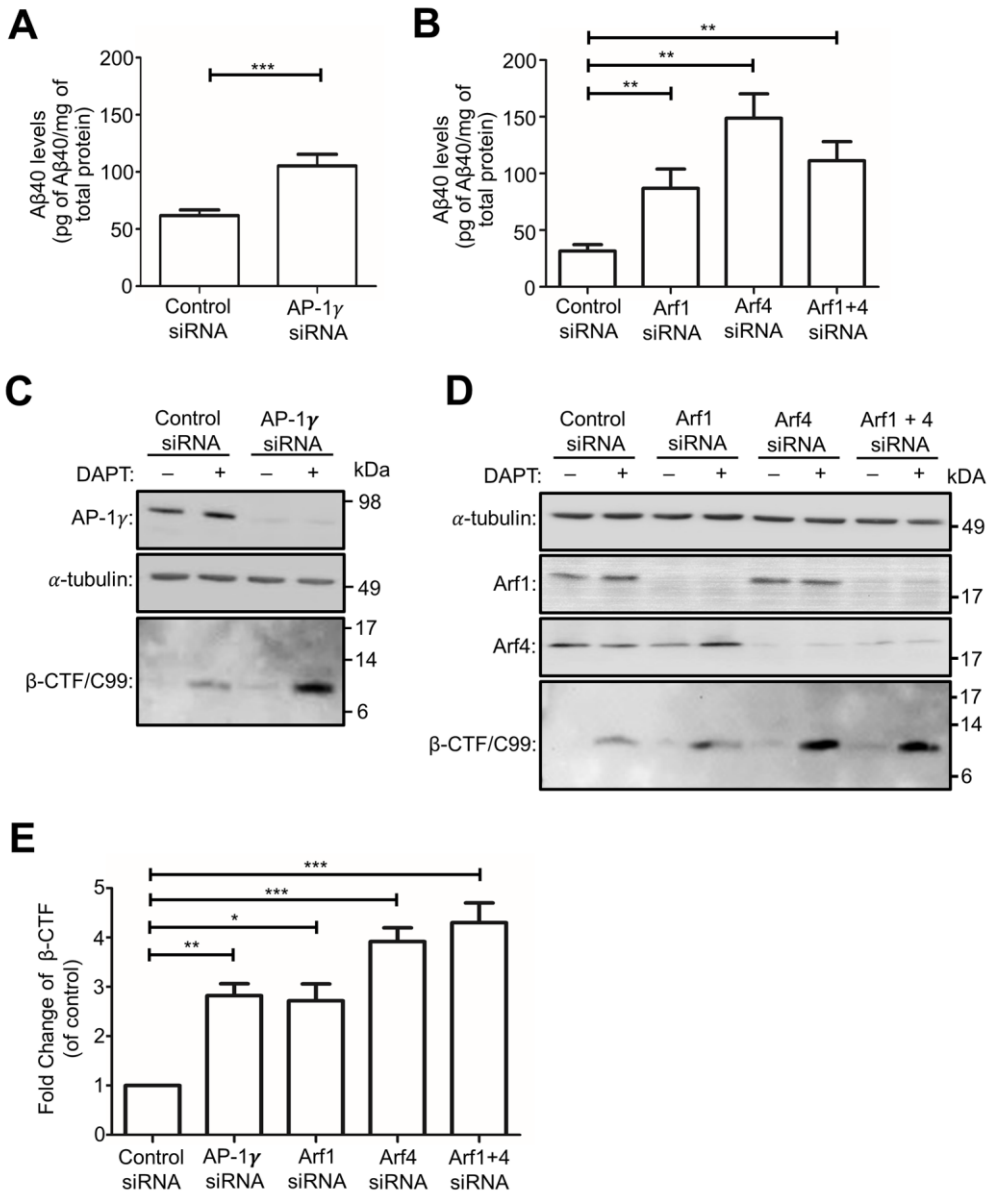
A
Aβ40 levels (pg of Aβ40/mg of total protein)
200
150
100
50
0
***
Control siRNA
AP-1γ siRNA
B
Aβ40 levels (pg of Aβ40/mg of total protein)
200
150
100
50
0
**
**
**
Control siRNA
Arf1 siRNA
Arf4 siRNA
Arf1+4 siRNA
C
Control siRNA
AP-1γ siRNA
DAPT: – + – +
kDa
AP-1γ:
α-tubulin:
β-CTF/C99:
98
49
17
14
6
D
Control siRNA
Arf1 siRNA
Arf4 siRNA
Arf1 + 4 siRNA
DAPT: – + – + – + – +
kDA
α-tubulin:
Arf1:
Arf4:
β-CTF/C99:
49
17
17
17
14
6
E
Fold Change of β-CTF (of control)
5
4
3
2
1
0
***
***
*
**
Control siRNA
AP-1γ siRNA
Arf1 siRNA
Arf4 siRNA
Arf1+4 siRNA

Figure 11 Depletion of* AP-1γ *in mouse primary cortical neurons results in increased APP processing

(**A**) E16 primary mouse cortical neurons were transduced at DIV3 with either AP-1γ-shRNA1 or AP-1γ-shRNA2 lentivirus (LV) for 96 h, and treated with either DMSO (carrier control), 2 μM DAPT and/or 2 μM BACE1 inhibitor C3 in the last 16-20 h of transduction. Neurons were lysed in RIPA buffer and cell extracts (10 μg) subjected to SDS-PAGE, as described in Materials and Methods. Proteins transferred onto PVDF membrane were probed with mouse antibodies to either AP-1γ or α-tubulin. Proteins transferred onto nitrocellulose membrane were probed with rabbit anti-APP (Y188) antibodies to C99*/C83**.

(**B-D**) Bar graph representing percentage of (**B**) AP-1 depletion, and fold change of (**C**) β-CTF/C99 and (**D**) α-CTF/C83 in AP-1γ shRNA1 or AP-1γ shRNA2 lentiviral transduction compared to non-transduced controls. Levels of α-CTF/C83 and β-CTF/C99 were normalized to α-tubulin. (**B-D**) Data are represented as the mean ± SD of 3 independent experiments and analyzed by one-way ANOVA using Tukey's test. **$p<0.01$, *$p<0.05$, and n.s. = not significant.

(**E and F**) Primary mouse cortical neurons were transduced at DIV3 with either AP-1γ-shRNA1 or AP-1γ-shRNA2 lentivirus, and 80 h after transduction the medium changed and spent medium containing secreted Aβ collected 16 h later and analyzed with a sandwich ELISA specific for either (**E**) $A\beta_{40}$ or (**F**) $A\beta_{42}$. The $A\beta_{40}$ or $A\beta_{42}$ levels for each sample were normalized against the total cellular protein. Data are represented as the mean ± SEM of 3 independent experiments and analyzed by one-way ANOVA using Tukey's test. ***$p<0.001$, **$p<0.01$ and *$p<0.05$.

(**G**) *Model of anterograde transport pathway of newly synthesized APP and BACE1*. Both BACE1 (green bars) and APP (red bars) are synthesized in the ER and transported through the Golgi. Upon arrival at the TGN, APP and BACE1 are sorted by distinct transport machinery for TGN export. BACE1 is transported from the TGN directly to the PM via an AP-1/Arf1/Arf4 dependent pathway. APP is transported via an AP-4/Arl5b dependent pathway from the TGN directly to the early endosomes then to either the PM or the late endosomes/lysosomes

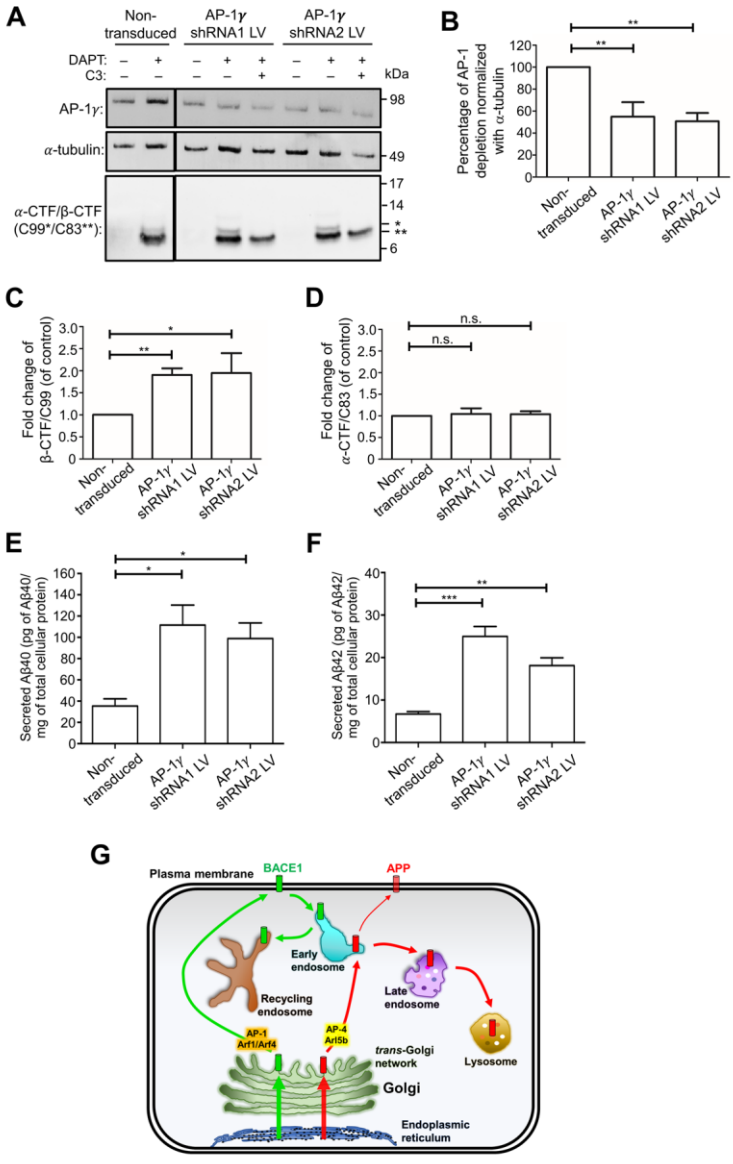
A
Non-transduced
AP-1γ shRNA1 LV
AP-1γ shRNA2 LV
DAPT:
C3:
kDa
AP-1γ:
α-tubulin:
α-CTF/β-CTF (C99*/C83**):
98
49
17
14
6
B
Percentage of AP-1 depletion normalized with α-tubulin
C
Fold change of β-CTF/C99 (of control)
D
Fold change of α-CTF/C83 (of control)
n.s.
E
Secreted Aβ40 (pg of Aβ40/ mg of total cellular protein)
F
Secreted Aβ42 (pg of Aβ42/ mg of total cellular protein)
G
Plasma membrane
BACE1
APP
Early endosome
Recycling endosome
Late endosome
Lysosome
AP-1 Arf1/Arf4
AP-4 Arl5b
trans-Golgi network
Golgi
Endoplasmic reticulum

Table 1: Steady-state distribution of BACE1 in HeLa cells and primary mouse cortical neurons

Organelles	**HeLa cells** (Transient expression)		**HeLa cells** (Stable expression)	**Primary mouse cortical neurons**
	Untagged-BACE1 (Chia *et al.*, 2013)	BACE1-SBP-GFP	BACE1-GFP	Endogenous BACE1
trans-Golgi network	4.4%	8.5%	5.6%	5.6%
Recycling endosomes	31.9%	30.6%	29.8%	40.7%
Early endosomes	31.8%	27.4%	21.0%	22.4%
Late endosomes/ Lysosomes	12.0%	9.7%	9.1%	15.5%

Table 2: Acidic cluster motifs in the cytoplasmic tails of membrane cargoes

Cargoes	Acidic cluster motif	Ref.
Furin	SDSEEDE	(Voorhees *et al.*, 1995)
Carboxypeptidase D	DETDTEEE	(Eng *et al.*, 1999)
Cation-independent mannose 6-phosphate receptor	DDQDSED and DDSDEDLL	(Chen *et al.*, 1997)
Dyslexia-associated protein KIAA0319-like protein	SESELDSDD	(Navarro Negredo *et al.*, 2017)
BACE1	DDFADDISLL	-